

NEW SELF-SIMILAR EULER FLOWS: GRADIENT CATASTROPHE WITHOUT SHOCK FORMATION

HELGE KRISTIAN JENSSEN AND ALEXANDER ANTHONY JOHNSON

ABSTRACT. We consider self-similar solutions to the full compressible Euler system for an ideal gas in two and three space dimensions. The system admits a 2-parameter family of similarity solutions depending on parameters λ and κ . Requiring locally finite amounts of mass, momentum, and energy imply certain constraints on λ and κ . Further constraints are imposed for particular types of flows. E.g., Guderley's pioneering construction of an unbounded converging shock wave invading a quiescent fluid, requires $\kappa = 0$ and $\lambda > 1$.

In this work we analyze the regime $0 < \lambda < 1$, which does not appear to have been addressed previously. Our findings include: (i) non-existence of Guderley shock solutions; (ii) existence of bounded and continuous incoming similarity flows in 3-d provided κ takes the value $\hat{\kappa} = \frac{2(1-\lambda)}{\gamma-1}$, λ is sufficiently small, and γ is sufficiently large; (iii) continuation of the latter flows beyond collapse as globally defined and continuous similarity solutions.

A key feature of these solutions is that they, in contrast to Guderley solutions, remain bounded at time of collapse, while the density, velocity, and sound speed all suffer gradient blowup. It is noteworthy that, notwithstanding infinite gradients at collapse, no shock wave appears. The analysis is based on a combination of analytical and numerical calculations.

Key words. Compressible fluid flow, multi-d Euler system, radial symmetry, similarity solutions, singularity formation

AMS subject classifications. 35L45, 35L67, 76N10, 35Q31

CONTENTS

1. Introduction	2
1.1. Self similar Euler flows	2
1.2. Outline and main results	4
2. Critical points	7
2.1. Critical points P_1 - P_3	8
2.2. Critical points P_4 - P_9	8
2.3. Critical points $P_{\pm\infty}$	11
3. Absence of Guderley solutions when $0 < \lambda < 1$	11
4. Restrictions on λ and κ	13
4.1. Restrictions from integral bounds	13
4.2. Restrictions from pointwise bounds in a continuous flow	14
4.3. Isentropic behavior near $r = 0$	15
5. Construction of continuous flows with $0 < \lambda < 1$ and $\kappa = \hat{\kappa}$	16
5.1. Outline of construction	16
5.2. Location of critical points	17
5.3. The critical point $P_{+\infty}$	19
5.4. Behavior near P_8 ; construction of Γ_1	19
5.5. Behavior near P_1 ; construction of Γ_2	23

Date: June 1, 2022.

5.6. Summary	24
5.7. Numerical verification of (i) and (ii)	24
5.8. The flow at collapse and absence of shocks	25
Acknowledgements	27
References	28

1. INTRODUCTION

The non-isentropic (full) compressible Euler system expresses conservation of mass, momentum, and energy in fluid flow in the absence of second order effects:

$$\rho_t + \operatorname{div}_{\mathbf{x}}(\rho \mathbf{u}) = 0 \quad (1.1)$$

$$(\rho \mathbf{u})_t + \operatorname{div}_{\mathbf{x}}[\rho \mathbf{u} \otimes \mathbf{u}] + \operatorname{grad}_{\mathbf{x}} p = 0 \quad (1.2)$$

$$(\rho E)_t + \operatorname{div}_{\mathbf{x}}[(\rho E + p) \mathbf{u}] = 0. \quad (1.3)$$

The independent variables are time t and position $\mathbf{x} \in \mathbb{R}^n$, and the primary dependent variables are density ρ , fluid velocity \mathbf{u} , and internal energy e ; the total energy density is $E = e + \frac{1}{2}|\mathbf{u}|^2$. We restrict attention to ideal gases with pressure p given by

$$p(\rho, e) = (\gamma - 1)\rho e. \quad (1.4)$$

Throughout, the adiabatic constant γ is assumed to satisfy $\gamma > 1$. The local speed of sound c is

$$c = \sqrt{\frac{\gamma p}{\rho}} = \sqrt{\gamma(\gamma - 1)e}. \quad (1.5)$$

We consider radial flows in space dimension $n = 2$ or $n = 3$, i.e., the flow variables depend on position only through the distance $r = |\mathbf{x}|$ to the origin, and the velocity field is purely radial, viz. $\mathbf{u} = u \frac{\mathbf{x}}{r}$. With these assumptions, and within smooth regions of the flow, (1.1)-(1.3) read

$$\rho_t + u\rho_r + \rho(u_r + \frac{m}{r}u) = 0 \quad (1.6)$$

$$u_t + uu_r + \frac{1}{\gamma\rho}(\rho c^2)_r = 0 \quad (1.7)$$

$$c_t + uc_r + \frac{\gamma-1}{2}c(u_r + \frac{m}{r}u) = 0, \quad (1.8)$$

where $\rho = \rho(t, r)$, $u = u(t, r)$, $c = c(t, r)$, and $m = n - 1$.

1.1. Self similar Euler flows. We next specialize further by imposing self similarity [9, 11, 25, 26]. For this we follow [9, 17] and introduce the similarity variables

$$x = \frac{t}{r^\lambda}, \quad \rho(t, r) = r^\kappa R(x), \quad u(t, r) = -\frac{r^{1-\lambda}}{\lambda} \frac{V(x)}{x}, \quad c(t, r) = -\frac{r^{1-\lambda}}{\lambda} \frac{C(x)}{x}. \quad (1.9)$$

At this stage the similarity parameters λ and κ are free.

Substitution of (1.9) into (1.6)-(1.7) yield three coupled ODEs for $R(x)$, $V(x)$, $C(x)$. The density variable R can be eliminated to give two coupled ODEs for only V and C , viz.

$$\frac{dV}{dx} = -\frac{1}{\lambda x} \frac{G(V, C)}{D(V, C)} \quad (1.10)$$

$$\frac{dC}{dx} = -\frac{1}{\lambda x} \frac{F(V, C)}{D(V, C)}, \quad (1.11)$$

which in turn yield a single, autonomous ODE

$$\frac{dC}{dV} = \frac{F(V, C)}{G(V, C)} \quad (1.12)$$

relating V and C along self-similar solutions. The functions D , G , F are given by

$$D(V, C) = (1 + V)^2 - C^2 \quad (1.13)$$

$$G(V, C) = nC^2(V - V_*) - V(1 + V)(\lambda + V) \quad (1.14)$$

$$F(V, C) = C \left\{ C^2 \left(1 + \frac{\alpha}{1+V} \right) - k_1(1 + V)^2 + k_2(1 + V) - k_3 \right\}, \quad (1.15)$$

where

$$V_* = \frac{\kappa - 2(\lambda - 1)}{n\gamma}, \quad (1.16)$$

$$\alpha = \frac{1}{2\gamma} [\kappa(\gamma - 1) + 2(\lambda - 1)], \quad (1.17)$$

and

$$k_1 = 1 + \frac{(n-1)(\gamma-1)}{2}, \quad k_2 = \frac{(n-1)(\gamma-1) + (\gamma-3)(\lambda-1)}{2}, \quad k_3 = \frac{(\gamma-1)(\lambda-1)}{2}. \quad (1.18)$$

Evidently, the construction of radial self-similar Euler flows requires an analysis of the phase portrait for (1.12) in the (V, C) -plane. However, since the ODEs (1.10)-(1.11) are singular along the two critical lines defined by $D(V, C) = 0$, only certain trajectories of (1.12) yield physically meaningful flows. Specifically, any trajectory crossing a critical line can do so only at points where all three of F , G , and D vanish.

Having identified an admissible trajectory Γ of (1.12) connecting some of its equilibria, it may be used to generate a solution to the system (1.10)-(1.11). Finally, it must be checked that the resulting solution $(V(x), C(x))$ moves along Γ in the correct manner as x increases from $-\infty$ to $+\infty$. In particular, this is an issue for the solutions we construct. These pass through the origin in the (V, C) -plane for $x = 0$ and it must be verified that the signs of F , G , D , and x match up correctly at the crossing. E.g., the physical requirement that sound speed is non-negative implies that the solution passes from $\{C > 0\}$ to $\{C < 0\}$ as x increases from negative to positive values.

The analysis of (1.12) involves a fair amount of calculations as the number, locations, and types of its equilibria depend on the parameters n , γ , λ , and κ . In Section 2 we record the explicit expressions for the equilibria, valid for any choice of parameters. Since we have not found it in the existing literature, we also provide a complete breakdown of when the various equilibria of (1.12) are present.

Once a solution to (1.10)-(1.11) has been selected, the velocity and sound speed in the corresponding Euler flow are determined via (1.9). The full description of the flow requires also the density field $\rho(t, r) = r^\kappa R(x)$. This can be obtained within each region of continuous flow from the following explicit *entropy integral*

$$\left(\frac{C(x)}{x} \right)^2 R(x)^{1-\gamma} [R(x)|1 + V(x)|]^q \equiv \text{constant} > 0, \quad (1.19)$$

with $R \geq 0$ and

$$q = \frac{1}{\kappa+n} [\kappa(\gamma - 1) + 2(\lambda - 1)] = \frac{2\gamma}{\kappa+n} \alpha. \quad (1.20)$$

The existence of this integral is a consequence of the fact that the specific entropy remains constant along particle trajectories in continuous Euler flow.

For later reference we note that the choice

$$\kappa = \hat{\kappa} := \frac{2(1-\lambda)}{\gamma-1}, \quad (1.21)$$

makes α , and hence q vanish. The entropy integral (1.19) then reduces to

$$\left(\frac{C(x)}{x} \right)^2 R(x)^{1-\gamma} \equiv \text{constant} > 0. \quad (1.22)$$

In terms of temperature $\theta \propto c^2$ and density ρ , this amounts to $\theta \rho^{1-\gamma}$ being constant, i.e., the specific entropy takes a constant value throughout any region of continuity. Thus, continuous similarity flows with $\kappa = \hat{\kappa}$ provide isentropic solutions to the Euler system. The solutions we build in Section 5 are of this type.

1.2. Outline and main results. The present work addresses a particular type of converging-diverging flows with $\lambda \in (0, 1)$, in which an incoming radially symmetric wave collapses on the center of motion and reflects an outgoing wave. Without loss of generality, the time of collapse is chosen as $t = 0$, a choice which is built into the definition of the similarity variable x in (1.9).

Before describing our findings we briefly review some earlier results. The pioneering study [11] of Guderley provided examples of unbounded converging-diverging shock waves in an ideal gas. An incoming spherical shock wave approaches the origin by invading a quiescent fluid (homogeneous and at rest), while gaining strength. At collapse it has infinite speed and the velocity, sound speed, and pressure in its immediate wake are unbounded. The subsequent flow accommodates the infinite amplitudes at the center of motion by generating an expanding shock wave, which then slows down and weakens as it interacts with the still-incoming flow ahead of it.

In what follows, solutions in which a converging shock invades a quiescent fluid, collapses at the origin, and then generates an expanding shock wave, will be referred to as *Guderley solutions*. Their construction depends on resolving a nonlinear eigenvalue problem for the similarity parameter λ (see Section 3). It turns out that, in a Guderley solution, the similarity parameter κ must necessarily be zero and that the temperature in the quiescent part of the fluid vanishes identically. The allowed λ values depend on both the geometry (n) and the gas (γ), and are dictated by the requirement that a certain ODE-trajectory pass through a particular equilibrium of (1.12). Their determination must be done numerically, a task that has been carried out to considerable accuracy in a number of works (for $n = 2$ or 3 and various $\gamma > 1$); see [1, 3, 11–13, 17, 24] and references therein.

Remark 1.1. *In the applied literature on self-similar Euler flows the emphasis has been on Guderley solutions due to their relevance to inertial fusion research, [1, 10, 22, 23]. The closely related construction of unbounded self-similar cavity flows has been analyzed in [3, 14, 17].*

In all works on self-similar solutions to the Euler system that we are aware of, attention is restricted to similarity parameters $\lambda > 1$ or, as a limiting case, $\lambda = 1$ ¹. Our first objective in this work is to consider the possibility of Guderley shock solutions when $\lambda \in (0, 1)$. Since a shock in a similarity flow propagates along a path with $x = \frac{t}{r^\lambda} \equiv \text{constant}$, $\lambda \in (0, 1)$ would yield a “glancing” shock wave that weakens and slows down, reaching the center of motion with vanishing speed. However, as described in Section 3, it does not appear possible to generate a Guderley solution when $\lambda \in (0, 1)$: the relevant ODE-trajectories simply do not reach the required equilibrium.

We then turn to the possibility of constructing *continuous* self-similar radial Euler flows. For $\lambda > 1$ such solutions have recently been constructed, up to time of collapse, in the works [15, 16, 20]. These solutions suffer amplitude blowup at the $t = 0$ and are propagated to positive times in [15, 16] by having a shock emerge from the center of motion, similar to what occurs in Guderley solutions.

Remark 1.2. *The work [20] addresses the subtle issue of constructing smooth (C^∞) self-similar isentropic flows (up to collapse). The recent work [2] provides numerical evidence that these solutions are linearly unstable with respect to 1-d radial perturbations.*

We note that the continuous solutions considered in [15, 16, 20] demonstrate in particular that amplitude blowup does not require a central region of vanishing pressure, as is the case in Guderley solutions and cavity flows.

The main contribution of the present work is the construction and analysis of *globally* continuous radial self-similar flows for the full Euler system with similarity parameter $\lambda \in (0, 1)$. This parameter range yields very different behavior compared to those of Guderley solutions, or those in [15, 16, 20]: instead of suffering amplitude blowup, the primary flow variables ρ , u , c remain bounded near the center of motion, and instead suffer *gradient catastrophes* at time of collapse $t = 0$. However, notwithstanding the infinite gradients, the solutions propagate as *continuous* flows

¹We note that $\lambda = 1$ provides the setting for the study of multi-d Riemann problems, [27].

to positive times. We find it noteworthy that this can occur even in cases where all fluid particles move *toward* the origin at time $t = 0$.

The issue of shock formation and propagation in multi-d Euler flows has recently been analyzed in great detail, providing fundamental new results in the field, see [4–8, 18, 19] and references therein. In this connection, the solutions we obtain here simply point out that singularity formation (i.e., some of the primary flow variables suffer a gradient catastrophe), does not necessarily give rise to a shock wave; for further detail see Remark 1.5.

Remark 1.3. *We have not addressed the stability of the solutions we obtain. However, we note that their pressure fields do not suffer gradient blowup. In fact, at time of collapse the pressure vanishes super-linearly as $r \downarrow 0$ (see Section 4.3), which might provide a stabilizing effect.*

The construction of globally continuous self-similar flows with $\lambda \in (0, 1)$ follows the standard strategy of building solutions from trajectories of the ODE (1.12) connecting some of its equilibria. However, the requirements of continuity and $0 < \lambda < 1$ impose additional constraints. First, as in [16], we show that continuity of the flow (specifically, boundedness of ρ and c at the center of motion prior to collapse) requires the similarity parameter κ to take the “isentropic” value $\kappa = \hat{\kappa}$ in (1.21). As noted above, this choice renders the flow globally isentropic. We verify that it also guarantees the absence of a gradient catastrophe prior to $t = 0$ (Section 4.3).

In addition, to guarantee the existence of suitable trajectories when $\lambda \in (0, 1)$, further restrictions must be imposed. These are dictated by the requirement that a certain critical point (P_8 in what follows) be a proper node with a suitable primary direction. It turns out that this requires the space dimension to be 3, and that λ belongs to the restricted range $(0, \frac{1}{9})$. Finally, the adiabatic constant needs to be sufficiently large, viz. $\gamma > \gamma_3(\lambda)$, where the latter is an increasing function satisfying

$$\lim_{\lambda \downarrow 0} \gamma_3(\lambda) = \gamma_* \approx 8.72, \quad \lim_{\lambda \uparrow \frac{1}{9}} \gamma_3(\lambda) = +\infty;$$

see Figure 3. With these assumptions met, we verify numerically the existence of suitable ODE trajectories. Our main findings are as follows:

Main Results. *Consider radial self-similar solutions of the form (1.9) to the full multi-d Euler system (1.1)-(1.3) in space dimension 2 or 3, with similarity variables λ and κ . Then:*

- (1) *No Guderley solutions (converging shock invading a quiescent state) appear possible when $\lambda \in (0, 1)$.*
- (2) *The existence of continuous self-similar solutions requires that κ takes the “isentropic” value $\hat{\kappa}$ in (1.21); in turn, this choice renders the flow globally isentropic and without singularities (gradient catastrophes) prior to collapse.*
- (3) *With $\kappa = \hat{\kappa}$ there is a 1-parameter family of continuous self-similar solutions (1.9) which describe a converging wave collapsing at the origin at time $t = 0$. Our construction of this type of solution requires $n = 3$, $\lambda \in (0, \frac{1}{9})$, and sufficiently large values of γ , viz. $\gamma > \gamma_3(\lambda)$.*
- (4) *The solutions described in (3), while locally bounded, are such that ρ , u , c all suffer gradient catastrophes at the origin at time of collapse. The pressure is C^1 -smooth and vanishes super-linearly as the center of motion is approached at time $t = 0$.*
- (5) *Notwithstanding infinite gradients in ρ , u , and c at collapse, we provide examples of solutions that extend as continuous similarity solutions to positive times. Numerical evidence suggests that no outgoing shock is generated whenever λ and γ are as described in (3).*

Two remarks are in order.

Remark 1.4. *The solutions described in parts (3)-(5) have locally bounded mass, momentum, and energy. On the other hand, it is readily verified that they are unbounded as $r \rightarrow \infty$ at any fixed*

time \bar{t} ; specifically,

$$u(\bar{t}, r) \sim r^{1-\lambda}, \quad c(\bar{t}, r) \sim r^{1-\lambda} \quad \text{and} \quad \rho(\bar{t}, r) \sim r^{\hat{\kappa}} \quad \text{as } r \uparrow \infty. \quad (1.23)$$

Since $\lambda < 1$, the solutions have infinite total mass, momentum, and energy. However, it appears reasonable that the same local behavior near the center of motion can be obtained in solutions with bounded mass, momentum, and energy. This could be achieved by fixing a time $t_0 < 0$ and modifying the self-similar solution outside of a sufficiently large ball $B_{R_0}(0)$. Specifically, R_0 should be larger than the radial position $r_c(t_0)$, where $r_c(t)$ denotes the critical 1-characteristic (sonic curve) passing through the origin at $t = 0$. This would ensure that the modified part of the solution remain causally independent of the flow near $r = 0$, provided the modified solution remains continuous up to time $t = 0$. It is reasonable that this scenario can be achieved (e.g., by having the modification at time t_0 generate a suitable expanding rarefaction wave), but we stress that we do not have a rigorous proof of this.

Remark 1.5. Concerning the absence of shocks, it is of interest to consider the behavior of 1-characteristics near the center of motion in the continuous solutions described above. For this, fix a time $t_0 < 0$ and let $r(t, \xi)$ denote the 1-characteristic that passes through location $r = \xi$ at time t_0 , i.e.,

$$\partial_t r(t, \xi) = (u - c)|_{(t, r(t, \xi))}, \quad r(t_0, \xi) = \xi. \quad (1.24)$$

The critical 1-characteristic (sonic line) which arrives at the origin at time of collapse, propagates along the path $r_c(t) = |\frac{t}{x_8}|^{\frac{1}{\lambda}}$ for $t < 0$, where x_8 is the x -value for which the incoming solution passes through the particular critical point $P_8 \in \{D = 0\} \cap \{F = 0\} \cap \{G = 0\}$ (cf. (1.13)-(1.14)(1.15)). We are interested in the density of 1-characteristics at the center of motion at time $t = 0$. We therefore set

$$\mu(t, \xi) := \partial_\xi r(t, \xi),$$

and seek to compute $\mu(0, \xi_c)$, where $\xi_c = r_c(t_0)$. Shock formation is expected when the characteristics concentrate, i.e., $\mu(0, \xi_c) = 0$. Differentiating (1.24) with respect to ξ yields

$$\partial_t \log \mu(t, \xi) = (u_r - c_r)|_{(t, r(t, \xi))} = \frac{1}{\lambda t} [\lambda x(V'(x) - C'(x)) + (C(x) - V(x))].$$

For $\xi = \xi_c$, which corresponds to $x = x_8$, this gives

$$\partial_t \log \mu(t, \xi_c) = \frac{A_8}{\lambda t},$$

where the constant A_8 is given by

$$A_8 = \lambda x_8(V'(x_8) - C'(x_8)) + 1.$$

A_8 is explicitly available and is given in terms of the first partials of $F(V, C)$ and $G(V, C)$ at P_8 , and is a (somewhat complicated) function of λ and γ . Integrating from time t_0 to $t < 0$, and using $\mu(t_0, \xi) \equiv 1$, we have

$$\mu(t, \xi_c) = \left| \frac{t}{t_0} \right|^{\frac{A_8}{\lambda}}.$$

It follows that shock formation at the center of motion at time $t = 0$ would require $A_8 > 0$. However, a numerical evaluation reveals that $A_8 < 0$ whenever the parameters are as described in part (3) of the Main Results (i.e., $n = 3$, $\lambda \in (0, \frac{1}{9})$, and $\gamma > \gamma_3(\lambda)$). This provides an analytic verification of the absence of shocks in the constructed self-similar flows. An alternative, graphic verification based on the Rankine-Hugoniot relations is described in Section 5.8.

The rest of the article is organized as follows. In Section 2 we record the equilibria of (1.10)-(1.11). There are up to 11 of these and we provide a complete breakdown of their presence depending on the parameters n , γ , λ , and κ . The cases when $\kappa = 0$ and $\kappa = \hat{\kappa}$ are treated separately for later use. Section 3 describes Guderley solutions and argues that no such solution appears possible when $\lambda \in (0, 1)$. Turning to the construction of continuous similarity flows for this λ range, we make

use of the singular points at infinity ($P_{\pm\infty}$) and at the origin (P_1). For the resulting flows we then analyze the restrictions placed on λ and κ by integrability and continuity constraints. These are dealt with in Section 4 where it is found that the latter constraint fixes $\kappa = \hat{\kappa}$. We also verify that no gradient catastrophe occurs prior to collapse in the resulting flows.

The construction of the relevant trajectories is detailed in Section 5. For this we want that one of the critical points, P_8 , is a proper node, guaranteeing that an infinite number of trajectories are drawn to it. This requires a detailed analysis of various quantities defined in terms of the partial derivatives of F and G at P_8 . We then show how the requirement that the saddle point $P_{+\infty}$ be joined to the node at P_8 via a trajectory Γ_1 of (1.10)-(1.11) imposes the additional constraints $n = 3$, $\lambda \in (0, \frac{1}{9})$, and $\gamma > \gamma_3(\lambda)$ (Sections 5.3-5.4). We next describe how to select suitable trajectories Γ_2 joining P_8 to its reflection P_9 about the V -axis (Section 5.5). Such trajectories must pass through the proper node P_1 at the origin; there is typically an infinite number of such solutions. Finally, we add the reflection Γ_3 of Γ_1 about the V -axis to define the complete solution trajectory $\Gamma := \Gamma_1 \cup \Gamma_2 \cup \Gamma_3$ of (1.10)-(1.11). The corresponding flow variables defined via (1.9) and (1.22) then provide global, 3-dimensional, self-similar, and continuous Euler flows. Section 5.6 summarizes the construction and the required numeric tests, which are done in Section 5.7.

To illustrate the construction in Section 5, we provide figures displaying the various trajectories for the particular case $n = 3$, $\lambda = 0.02$, $\gamma = 12$. We finally illustrate graphically the absence of a shock wave in the flow after collapse in this case (Section 5.8).

2. CRITICAL POINTS

Throughout this section $n = 2$ or 3 , and $\gamma > 1$. The goal is to identify the critical points of (1.12) and to determine how their presence depends on the parameters κ and λ , which are unrestricted for now (until Section 2.2.3). As we have not found it in the existing literature, we provide a complete breakdown of all the cases.

Remark 2.1. *The presence of some of the critical points (viz. P_6 - P_9 in the notation introduced below) places certain constraints on the parameters λ , κ , γ , and n ; see Section 2.2. Further requirements are imposed in Section 4.*

We introduce the *critical lines*

$$\mathcal{L}_{\pm} := \{(V, C) \mid C = \pm(1 + V)\},$$

and note the relation

$$F(V, \pm(1 + V)) \equiv \mp \frac{(\gamma-1)}{2} G(V, \pm(1 + V)). \quad (2.1)$$

The critical points of (1.12) are the points of intersection between the zero-level sets

$$\mathcal{F} := \{(V, C) : F(V, C) = 0\} \quad \text{and} \quad \mathcal{G} := \{(V, C) : G(V, C) = 0\}$$

of the functions F and G defined in (1.15) and (1.14), respectively. Note that $V = V_*$ (see (1.16)) is a vertical asymptote for \mathcal{G} . The following symmetries will be important in assembling trajectories of (1.10)-(1.11),

$$G(V, -C) = G(V, C), \quad F(V, -C) = -F(V, C). \quad (2.2)$$

It turns out that there are up to nine points of intersection between \mathcal{F} and \mathcal{G} , and we follow [17] in numbering these $P_i = (V_i, C_i)$, $i = 1, \dots, 9$. In addition there are two critical points at infinity,

$$P_{\pm\infty} := (V_*, \pm\infty), \quad (2.3)$$

both of which are used in the construction of continuous Euler flows in Section 5.

2.1. Critical points P_1 - P_3 . We begin by observing that there are always three critical points located along the V -axis:

$$P_1 := (0, 0), \quad P_2 := (-1, 0), \quad \text{and} \quad P_3 := (-\lambda, 0).$$

Of these only P_1 is relevant for our purposes. The linearization of (1.12) at P_1 is $\frac{dC}{dV} = \frac{C}{V}$ (for all values of n , γ , κ , and λ), showing that P_1 is a star point (proper node). Thus, for any straight line ℓ from the origin, there is a unique trajectory $(V, C(V))$ of (1.12) which approaches the origin tangent to ℓ .

Assume now that a solution $(V(x), C(x))$ of (1.10)-(1.11) approaches P_1 with slope k . The corresponding trajectory $(V, C(V))$ of (1.12) then satisfies $C(V) \approx kV$ for $V \approx 0$, and an inspection of (1.10)-(1.11) yields

$$\frac{dV}{dx} \approx \frac{V}{x} \quad \text{and} \quad \frac{dC}{dx} \approx \frac{C}{x}$$

as P_1 is approached. It follows from this that any solution of (1.10)-(1.11) reaching P_1 must do so for $x = 0$, and also that the limits

$$\nu := \lim_{x \rightarrow 0} \frac{V(x)}{x} \quad \text{and} \quad \omega := \lim_{x \rightarrow 0} \frac{C(x)}{x} \quad \text{exist as finite numbers.} \quad (2.4)$$

This last property is a minimal requirement for (1.9) to yield a meaningful flow at time $t = 0$. (In the limiting case that P_1 is reached with infinite slope, ν vanishes.)

Observe also that due to the requirement that $c(t, r) \geq 0$, we get from (1.9) that a solution $(V(x), C(x))$ of (1.10)-(1.11) must necessarily pass from the upper half-plane $\{C > 0\}$ to the lower half-plane $\{C < 0\}$ as x increases from negative to positive values.

2.2. Critical points P_4 - P_9 . The critical points P_4 - P_9 are obtained by solving $G(V, C) = 0$ for C^2 in terms of V , and substituting the result into the equation $F(V, C) = 0$; this yields a cubic polynomial in V (see below). According to the symmetries in (2.2), the critical points P_4 - P_9 come in pairs located symmetrically about the V -axis. The ones located above (below) the V -axis are P_4 (P_5), P_6 (P_7), and P_8 (P_9). It turns out that among these, P_4 and P_5 are present for all values of n , κ , λ , and γ , while P_6 - P_9 may or may not be present.

Restricting attention to P_4 , P_6 , and P_8 , we proceed to determine when and where these occur. From $G(V, C) = 0$ we have

$$C^2 = \frac{V(1+V)(\lambda+V)}{n(V-V_*)}. \quad (2.5)$$

Substituting (2.5) into $F(V, C) = 0$, and recalling that we now seek critical points off the V -axis, give the following cubic equation for $W := 1 + V$:

$$\begin{aligned} [nk_1 - 1]W^3 - [nk_2 - \beta k_1 + \alpha + (\lambda - 2)]W^2 \\ + [nk_3 - \beta k_2 - (\lambda - 2)\alpha + (\lambda - 1)]W + [\beta k_3 + (\lambda - 1)\alpha] = 0, \end{aligned}$$

where α and the k_i are given in (1.17) and (1.18), and $\beta = -n(1 + V_*)$. This cubic always has one real root, denoted W_4 , and two possibly complex roots W_6 and W_8 . The root $W_4 = 1 + V_4$ is given by

$$V_4 = -\frac{\lambda}{1 + \frac{n}{2}(\gamma - 1)}, \quad (2.6)$$

(cf. Eqn. (3.3) in [17]). We note that V_4 is independent of κ ; however, the corresponding C -value $C_4 > 0$, given by (2.5), does depend on κ through V_* . The two remaining roots $V_6 \equiv V_-$ and $V_8 \equiv V_+$ are given by

$$V_{\pm} = \frac{1}{2m\gamma} \left[(\gamma - 2)\mu + \kappa - m\gamma \pm \sqrt{(\gamma - 2)^2\mu^2 - 2[\gamma m(\gamma + 2) - \kappa(\gamma - 2)]\mu + (\gamma m + \kappa)^2} \right], \quad (2.7)$$

where we have set

$$m := n - 1 \quad \text{and} \quad \mu := \lambda - 1. \quad (2.8)$$

(In what follows we use either λ or μ , always assuming $\mu = \lambda - 1$.) The values V_{\pm} , when real, yield the critical points $P_6 = (V_6, C_6)$ and $P_8 = (V_8, C_8)$ above the V -axis via (2.5). We record the non-obvious fact that

$$C_i^2 = (1 + V_i)^2 \quad \text{for } i = 6, 8. \quad (2.9)$$

Therefore, whenever P_6 and P_8 are present, they are necessarily located on one of the critical lines \mathcal{L}_{\pm} . By symmetry, the same applies to P_7 and P_9 .

We proceed to determine when the critical points P_6 and P_8 are present. This amounts to deciding when V_{\pm} are real, i.e., when the radicand in (2.7) is non-negative. To do so we consider two situations: either κ is a free parameter, or $\kappa = \hat{\kappa}$ is given in terms of λ and γ by (1.21). We start with the general case where κ is independent of λ , γ , and n .

2.2.1. General case: κ free. Consider the radicand in (2.7) as a polynomial in $\mu = \lambda - 1$; to organize the analysis we consider four sub-cases:

- (i) For $\gamma = 2$ the radicand in (2.7) is linear in μ , with the single root corresponding to

$$\lambda = \lambda_{\max} := 1 + \frac{(2m+\kappa)^2}{16m}. \quad (2.10)$$

In this case, V_{\pm} are real if and only if $\lambda \leq \lambda_{\max}$. The limiting case $\lambda = \lambda_{\max}$ yields $V_+ = V_- = \frac{\kappa}{4m} - \frac{1}{2}$.

Next, a direct calculation shows that for $\gamma \neq 2$ the radicand in (2.7) has the roots

$$\lambda = 1 + \frac{(m\gamma+\kappa)^2}{\left(\gamma\sqrt{m} \pm \sqrt{2\gamma m - \kappa(\gamma-2)}\right)^2}. \quad (2.11)$$

Here the \pm signs are unrelated to those in (2.7). The expressions in (2.11) generalize the expressions recorded by Lazarus who treated the cases $\kappa = 0$ and $\kappa = \hat{\kappa}$ (Section 3 in [17]).

- (ii) When $\gamma \neq 2$ and the radicand $2\gamma m - \kappa(\gamma-2)$ in (2.11) is strictly negative, then the radicand in (2.7) has no real μ -root. Therefore, since the coefficient of μ^2 in (2.7) is positive, the radicand in (2.7) is then strictly positive. Consequently, V_{\pm} are necessarily real and distinct numbers in this case.

If $\gamma \neq 2$ and the radicand in (2.11) satisfies $2\gamma m - \kappa(\gamma-2) \geq 0$, there are two further sub-cases depending on whether the minus-sign in (2.11) gives a vanishing denominator:

- (iii) When $\gamma \neq 2$ and $\kappa = -\gamma m$ (in particular, the radicand in (2.11) is strictly positive, but the minus-sign gives a $\frac{0}{0}$ expression), substitution of the latter κ -value directly into (2.7) gives

$$V_{\pm} = \frac{1}{2m\gamma} \left[(\gamma-2)\mu - 2m\gamma \pm \sqrt{(\gamma-2)^2\mu^2 - 4\gamma^2 m\mu} \right]. \quad (2.12)$$

In this case V_{\pm} are real numbers if and only if $\mu \leq 0$ or $\mu \geq \frac{4m\gamma^2}{(\gamma-2)^2}$, i.e., if and only if

$$\lambda \leq \lambda_{\max} := 1 \quad \text{or} \quad \lambda \geq \lambda_{\min} := 1 + \frac{4m\gamma^2}{(\gamma-2)^2}. \quad (2.13)$$

We have that $V_+ = V_-$ if and only if λ takes one of the values λ_{\min} or λ_{\max} .

- (iv) Finally, consider the case when $\gamma \neq 2$, $\kappa \neq -\gamma m$, and the radicand $2\gamma m - \kappa(\gamma-2)$ in (2.11) is non-negative. We set

$$\lambda_{\max} := 1 + \frac{(m\gamma+\kappa)^2}{\left(\gamma\sqrt{m} + \sqrt{2\gamma m - \kappa(\gamma-2)}\right)^2}, \quad (2.14)$$

and

$$\lambda_{\min} := 1 + \frac{(m\gamma+\kappa)^2}{\left(\gamma\sqrt{m} - \sqrt{2\gamma m - \kappa(\gamma-2)}\right)^2}, \quad (2.15)$$

so that V_{\pm} are real if and only if, either

$$\lambda \leq \lambda_{\max} \quad \text{or} \quad \lambda \geq \lambda_{\min}.$$

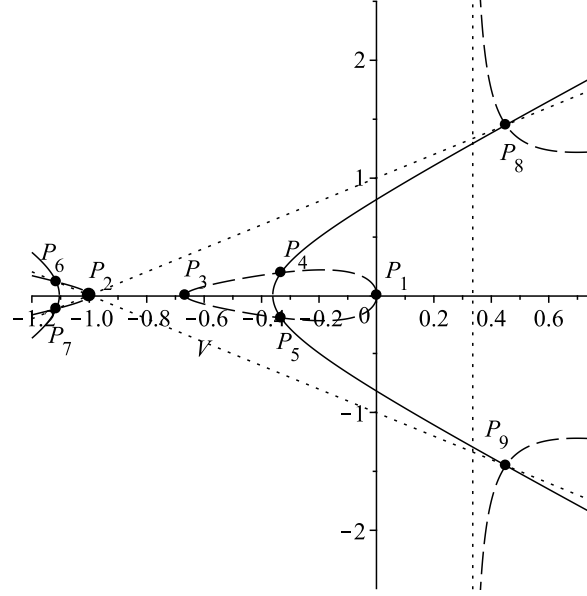


FIGURE 1. The zero-level curves of $F(V, C)$ (solid, including the V -axis) and $G(V, C)$ (dashed), together with the critical lines $\mathcal{L}_{\pm} = \{C = \pm(1 + V)\}$ and the vertical asymptote $V = V_*$ (dotted). The parameters are $n = 3$, $\gamma = \frac{5}{3}$, $\lambda = \frac{2}{3}$, and $\kappa = \hat{\kappa} = 1$. All of the singular points P_1 - P_9 are present in this case (solid dots).

Again, $V_+ = V_-$ if and only if λ takes one of the values λ_{\min} or λ_{\max} .

2.2.2. *The case $\kappa = 0$.* For later use we consider separately the case when $\kappa = 0$. V_{\pm} are then real provided

$$\lambda \leq \lambda_{\max} = 1 + \frac{m\gamma}{(\sqrt{\gamma} + \sqrt{2})^2} \quad \text{or} \quad \lambda \geq \lambda_{\min} = 1 + \frac{m\gamma}{(\sqrt{\gamma} - \sqrt{2})^2}.$$

For the special value $\gamma = 2$, we have V_{\pm} real whenever

$$\lambda \leq \lambda_{\max} = 1 + \frac{m}{4}.$$

Note that when $\kappa = 0$, we necessarily have $\lambda_{\max} > 1$.

2.2.3. *Isentropic case: $\kappa = \hat{\kappa}$.* In this case κ is fixed according to (1.21) for given λ and γ . In terms of $\mu = \lambda - 1$ we have

$$\hat{\kappa} = -\frac{2\mu}{\gamma-1},$$

and substitution of this κ -value into (2.7) gives

$$V_{\pm} = \frac{1}{2}(a \pm \sqrt{Q}), \quad (2.16)$$

where

$$a = \frac{(\gamma-3)}{m(\gamma-1)}\mu - 1 \quad \text{and} \quad Q = \left(\frac{(\gamma-3)}{m(\gamma-1)}\right)^2 \mu^2 - 2\frac{(\gamma+1)}{m(\gamma-1)}\mu + 1. \quad (2.17)$$

To have V_{\pm} real requires $Q \geq 0$. Regarding Q as a polynomial in μ there are two cases:

- (a) When $\gamma = 3$, Q is linear in μ and $Q \geq 0$ if and only if $\mu \leq \frac{m}{4}$. In terms of λ this means that V_{\pm} are real if and only if $\lambda \leq \lambda_{\max} := 1 + \frac{m}{4}$. Also, $V_- = V_+$ if and only if $\lambda = \lambda_{\max}$.
- (b) For $\gamma \neq 3$, Q is a quadratic in μ with a positive leading coefficient. A direct calculation shows that $Q \geq 0$ if and only if, either $\lambda \leq \lambda_{\max}$ or $\lambda \geq \lambda_{\min}$, where

$$\lambda_{\max} = 1 + \frac{m(\gamma-1)}{(\gamma+1) + \sqrt{8(\gamma-1)}} \quad (2.18)$$

and

$$\lambda_{\min} = 1 + \frac{m(\gamma-1)}{(\gamma+1)-\sqrt{8(\gamma-1)}}. \quad (2.19)$$

Finally, $V_+ = V_-$ if and only if λ takes one of the values λ_{\min} or λ_{\max} .

We note that, in either case (a) or case (b), $\lambda_{\max} > 1$ holds due to our assumptions $n \geq 2$ and $\gamma > 1$. In particular, when $\kappa = \hat{\kappa}$, P_6 and P_8 are present whenever $\lambda < 1$.

Figure 1 displays a representative case with $\kappa = \hat{\kappa}$ and all critical points present.

2.3. Critical points $P_{\pm\infty}$. The critical points at infinity are $P_{\pm\infty} = (V_*, \pm\infty)$. To analyze these we consider $P_{+\infty}$ (sufficient according to (2.2)) and change to the variables $W := V - V_*$ and $Z := C^{-2}$. Linearizing the resulting equation for $\frac{dZ}{dW}$ about $(W, Z) = (0, 0)$ yields

$$\frac{dZ}{dW} = -\frac{AZ}{nW - BZ}, \quad (2.20)$$

where

$$A = 2(1 + \frac{\alpha}{1+V_*}), \quad B = V_*(1 + V_*)(\lambda + V_*). \quad (2.21)$$

For later reference we note that $P_{+\infty}$ is a saddle point if and only if $A > 0$. The latter condition is satisfied when $\kappa = \hat{\kappa}$, since α then vanishes (see (1.17) and (1.21)).

3. ABSENCE OF GUDERLEY SOLUTIONS WHEN $0 < \lambda < 1$

Recall from Section 1.2 that a *Guderley solution* refers to a radial self-similar solution of the form (1.9) to the Euler system (1.6)-(1.8), defined (at least) for all negative times, and in which a converging shock wave approaches the origin by propagating into a quiescent fluid near the center of motion (i.e., the fluid is at rest and at constant pressure and density there).

It is further assumed that the parameters κ and λ are the same inside and outside of the converging shock, and that the shock follows a path with $x = \frac{t}{r^\lambda} \equiv x_s$, where x_s is a negative constant. As pointed out by Lazarus [17], the constant density inside the converging shock implies that the parameter κ must be zero for a Guderley solution. In this work we assume $\lambda \neq 1$, and it follows from (1.9) that the sound speed c must vanish within the quiescent region $x < x_s$. For the case of an ideal gas, this means that the temperature vanishes identically there. (We stress that the density within the quiescent region does not vanish in a Guderley solution; the collapse of a spherical vacuum region is a different problem which also admits similarity solutions, [3, 14, 17].) Therefore, for a Guderley solution, we have $(V(x), C(x)) \equiv (0, 0)$ for $-\infty < x < x_s$.

To the best of our knowledge, starting with [11], all works on Guderley solutions assume that $\lambda \geq 1$. In order that the shock accelerates and collapses with infinite speed one must have $\lambda > 1$. Among the many works on Guderley solutions (and collapsing cavities) we have found only a few that address the choice of range for λ . Among these, [14, 17] simply choose to disregard cases where the shock collapses with vanishing speed, while [3] (p. 16) claims that $\lambda < 1$ “is incompatible with any finite pressure before the wave.” However, we do not see any *a priori* reason to exclude cases with $0 < \lambda < 1$. If the Euler system admitted converging similarity shocks for this range, they would provide examples of “glancing” shocks that weaken, slow down, and reach the origin with zero speed.

However, based on numerical tests, we conjecture that the Euler system (for an ideal gas in 2 or 3 space dimensions) does not admit Guderley solutions with this type of glancing similarity shock. In the rest of this section we briefly describe the analysis leading to this conclusion. Thus, for the remainder of this section, the assumptions

$$0 < \lambda < 1 \quad \text{and} \quad \kappa = 0$$

are in force. First, the Rankine-Hugoniot relations for a discontinuity propagating in a similarity solution along a curve $x \equiv x_s$ in the (r, t) -plane are

$$1 + V_+ = \frac{\gamma-1}{\gamma+1}(1 + V_-) + \frac{2C_-^2}{(\gamma+1)(1+V_-)} \quad (3.1)$$

$$C_+^2 = C_-^2 + \frac{\gamma-1}{2}[(1 + V_-)^2 - (1 + V_+)^2] \quad (3.2)$$

$$R_+(1 + V_+) = R_-(1 + V_-), \quad (3.3)$$

where the subscripts $-$ and $+$ refer to states immediately prior to and after passing through the shock, respectively. Note that, in a Guderley solution the converging shock invades a quiescent state where $(V_-, C_-) = (0, 0)$, and it follows from (3.1)-(3.2) that

$$P_+ = (V_+, C_+) = \left(-\frac{2}{\gamma+1}, \frac{\sqrt{2\gamma(\gamma-1)}}{\gamma+1}\right). \quad (3.4)$$

Note that P_+ depends only on γ and is located on the graph of the function $C_+(V) := \sqrt{(1+V)(2+V)}$ for $-1 < V < 0$.

Next, the entropy conditions for a converging similarity 1-shock defined for negatives times take the form

$$C_- < 1 + V_- \quad \text{and} \quad C_+ > 1 + V_+. \quad (3.5)$$

(It may be shown from the entropy conditions that any converging self-similar shock with a quiescent inner state is necessarily a 1-shock when $\lambda > 0$.) As is evident from (3.4), P_+ is located above the critical line \mathcal{L}_+ , so that the 1-shock in a Guderley solution is entropy admissible.

To construct a Guderley solution (defined for all $t < 0$) it is then necessary to find a solution $(V(x), C(x))$ of (1.10)-(1.11) which starts out from P_+ with $x = x_s < 0$, and reaches the critical point P_1 at the origin with $x = 0$. In particular, it must cross the critical line \mathcal{L}_+ . Since the denominator $D(V, C)$ in (1.10)-(1.11) vanishes there, the only possibility is that the trajectory crosses at one of the critical points P_6 or P_8 ². For fixed $n = 2$ or 3 and $\gamma > 1$ it turns out that only certain values of λ makes this happen.

This non-linear eigenvalue problem for λ was first addressed by Guderley [11], and later by several authors, see [24]. As far as we know, the most comprehensive treatment (always for $\lambda \geq 1$) is due to Lazarus [17], who also carried out detailed numerical calculations. One conclusion of these works is that, for $n = 2$ or 3 and $\gamma > 1$, there is always at least one λ -value $\lambda > 1$ for which the trajectory starting at P_+ passes through either P_6 or P_8 , and then proceeds to reach $P_1 = (0, 0)$. (In fact, depending on γ , there can be whole intervals of allowed λ -values; also, once P_6 or P_8 has been reached from P_+ , there may be infinitely many trajectories connecting to the origin; see [17].)

With this background we now turn to the possibility of generating a Guderley solution when $0 < \lambda < 1$. As $\kappa = 0$ it follows from Section 2.2.2 that $V_6 = V_-$ and $V_8 = V_+$ are real, so that the critical points P_6, P_8 are necessarily present. A direct calculation using (2.6) and (2.7) shows that

$$V_6 < -1 < -\lambda < V_4 < 0 < V_* < V_8$$

in this case. (We omit the details; similar computations are detailed in the proof Lemma 5.1 below.) It follows that P_6 is located to the left of the vertical line $V = -1$, and therefore belongs to \mathcal{L}_- , while P_8 is located to the right of the vertical asymptote $V = V_*$ of \mathcal{G} , and lies on \mathcal{L}_+ . Also, in the case under consideration, $0 < C_4 < 1 + V_4$, so that P_4 is located strictly below \mathcal{L}_+ .

Let Γ_+ denote the sought-for trajectory (i.e., starting at P_+ and ending at $P_1 = (0, 0)$). Since $x < 0$ along Γ_+ , and since its starting point P_+ lies above \mathcal{L}_+ , it follows from (1.10)-(1.11) that the trajectory moves in the direction of the vector field $(-G(V, C), -F(V, C))$ as x increases from $x_s < 0$ toward 0. It may be verified that $G(V, C) < 0$ whenever (V, C) belongs to the region

²See (2.9). There is an apparent third possibility in the exceptional case that P_4 happens to lie on \mathcal{L}_+ . However, this is not a separate case: it can be shown that if $P_4 \in \mathcal{L}_+$, then P_4 necessarily coincides with either P_6 or P_8 .

$\mathcal{R} := \{-1 < V < 0 \text{ and } C > 1 + V\}$. Since Γ_+ starts at $P_+ \in \mathcal{R}$, it starts out moving to the right, and it follows that the only possibility for Γ_+ to reach P_1 is by crossing \mathcal{L}_+ at P_8 .

An inspection of the ODE system (1.10)-(1.11) shows that, depending on the value of $\gamma > 1$, this could potentially happen in one of two ways:

- (A) either P_+ is located near $P_2 = (-1, 0)$ and above $\mathcal{F} = \{(V, C) : F(V, C) = 0\}$ (this happens for γ -values sufficiently close to 1), and Γ_+ would start out by moving up in a North-East direction, then cross \mathcal{F} horizontally, before moving down in a South-East direction toward P_8 ; or,
- (B) P_+ is located below \mathcal{F} , and Γ_+ would move monotonically in a South-East direction toward P_8 . (This could only occur for γ sufficiently large, so that P_+ is located above P_8 .)

However, numerical tests with various choices for $\lambda \in (0, 1)$ and $\gamma > 1$ indicate that neither of these scenarios actually occurs. In all cases we have considered the trajectory Γ_+ hits \mathcal{L}_+ well to the left of P_8 . To have Γ_+ reach P_8 it appears advantageous to choose $\gamma \gg 1$, so that $P_+ \approx (0, \sqrt{2})$ is as close as possible to P_8 . However, even with extreme values for γ (of order 10^6 , say), we have not been able to find cases where Γ_+ even crosses into the right half-plane (where P_8 is located) before hitting \mathcal{L}_+ .

We therefore abandon the search for Guderley solutions when $\lambda \in (0, 1)$, and instead turn to the construction of *shock-free* solutions for this parameter regime. To do so we first need to consider constraints imposed on the similarity parameters λ, κ .

4. RESTRICTIONS ON λ AND κ

In this section the similarity parameters λ and κ are at the outset free, while $\gamma > 1$ is fixed and $n = 2, 3$. The goal is to obtain restrictions on λ and κ from physically relevant constraints as described below. Some of the arguments in this section are similar to those in [16]; for completeness we include the details.

4.1. Restrictions from integral bounds. Referring to the discussion in Section 2.1 we restrict attention to solutions $(V(x), C(x))$ of (1.10)-(1.11) which pass through the origin with (2.4) satisfied. It follows from (1.9) that the flow variables at time of collapse are given by

$$\rho(0, r) = R(0)r^\kappa \quad u(0, r) = -\frac{\nu}{\lambda}r^{1-\lambda}, \quad c(0, r) = -\frac{\mu}{\lambda}r^{1-\lambda}. \quad (4.1)$$

As a minimal, physical requirement we insist that the resulting flow has locally finite mass, momentum, and total energy, i.e., for each $\bar{r} > 0$, we have

$$\int_0^{\bar{r}} \rho(t, r) r^m dr, \quad \int_0^{\bar{r}} \rho(t, r) |u(t, r)| r^m dr, \quad \int_0^{\bar{r}} \rho(t, r) \left(e(t, r) + \frac{1}{2} |u(t, r)|^2 \right) r^m dr < \infty.$$

Using (4.1) it is straightforward to verify that, at time $t = 0$, these integral bounds imply

- (I) $\kappa + n > 0$
- (II) $\lambda < 1 + \kappa + n$
- (III) $\lambda < 1 + \frac{\kappa + n}{2}$,

respectively. Note that (II) is a consequence of (I) and (III). For later reference we record the following consequence: According to (III) and the standing assumption $\gamma > 1$, we have

$$0 < \frac{n + \kappa - 2(\lambda - 1)}{n\gamma} < \frac{n\gamma + \kappa - 2(\lambda - 1)}{n\gamma} = 1 + V_*. \quad (4.2)$$

4.2. Restrictions from pointwise bounds in a continuous flow. The restrictions (I)-(III) above are now in force; in particular, (4.2) holds. We then consider any solution $(V(x), C(x))$ of the similarity ODEs (1.10)-(1.11) which is defined for all $x < 0$, and with the property that it defines a *continuous* Euler flow for all $t < 0$. As far as we are aware, the only way for this to occur is by having the solution $(V(x), C(x))$ approach the critical point $P_{+\infty}$ in the upper half-plane:

$$(V(x), C(x)) \rightarrow P_{+\infty} = (V_*, +\infty) \quad \text{as } x \downarrow -\infty. \quad (4.3)$$

The latter property will hold, by construction, for the continuous solutions we analyze in Section 5, and (4.3) is assumed for the remainder of the present section.

Remark 4.1. *Strictly speaking, there may be another type of continuous similarity flows with $0 < \lambda < 1$ violating (4.3), viz. flows describing a spherical cavity (vacuum region) being filled by an inflowing gas. In this work we restrict attention to flows without open vacuum regions (but see Remark 4.2).*

By imposing continuity of the flow for $t < 0$, we require that the primary flow variables ρ , u , and c are locally bounded at any fixed time strictly prior to collapse. In particular, $\rho(\bar{t}, r)$, $u(\bar{t}, r)$, and $c(\bar{t}, r)$ should remain bounded as $r \downarrow 0$ whenever $\bar{t} < 0$. We proceed to analyze the implications of these requirements. For $\bar{t} < 0$ fixed we have

$$u(\bar{t}, r) = -\frac{r^{1-\lambda}}{\lambda} \frac{V(x)}{x} = -\frac{1}{\lambda \bar{t}} V(x) r \propto V(x) r.$$

From (4.3) it follows that $u(\bar{t}, r) \sim r$ as $r \downarrow 0$. This shows that the speed of the fluid particles, at any time $\bar{t} < 0$, approach zero at a linear rate as the center of motion is approached. Thus, no additional constraint is imposed on the similarity parameters λ and κ by requiring bounded (indeed, vanishing) fluid speed at the center of motion.

Next, to analyze $c(\bar{t}, r)$ as $r \downarrow 0$, we need the leading order behavior of $C(x)$ as $x \downarrow -\infty$. Applying (4.3) in (1.11) gives

$$\frac{1}{C} \frac{dC}{dx} \sim \frac{1}{\lambda} \left(1 + \frac{\alpha}{1+V_*}\right) \frac{1}{x} \quad \text{as } x \downarrow -\infty,$$

so that

$$C(x) \sim |x|^\sigma \quad \text{as } x \downarrow -\infty, \text{ where } \sigma = \frac{1}{\lambda} \left(1 + \frac{\alpha}{1+V_*}\right). \quad (4.4)$$

As \bar{t} is fixed, we have $x \propto -r^{-\lambda}$ and (1.9) gives

$$c(\bar{t}, r) \sim r^{1-\sigma\lambda} \quad \text{as } r \downarrow 0. \quad (4.5)$$

Boundedness of $c(\bar{t}, r)$ as $r \downarrow 0$ therefore imposes the constraint $1 - \sigma\lambda \geq 0$. According to (4.4) and (4.2), this amounts to $\alpha \leq 0$, or, according to (1.17),

$$2(\lambda - 1) + \kappa(\gamma - 1) \leq 0. \quad (4.6)$$

Next, to obtain the behavior of $\rho(\bar{t}, r)$ as $r \downarrow 0$, we use the exact integral (1.19) together with $V(x) \sim V_*$, $C(x) \sim |x|^\sigma$, and $x \propto r^{-\lambda}$, to get that

$$\rho(\bar{t}, r) \sim r^{\kappa + \frac{2\lambda(\sigma-1)}{1-\gamma+q}} \quad \text{as } r \downarrow 0, \quad (4.7)$$

where q is given by (1.20). Boundedness of $\rho(\bar{t}, r)$ as $r \downarrow 0$ therefore requires

$$\kappa + \frac{2\lambda(\sigma-1)}{1-\gamma+q} \geq 0. \quad (4.8)$$

We claim that (4.8), together with requirement (I) in Section 4.1, (4.2), and (4.6), imply that κ must take the “isentropic” value $\hat{\kappa}$ given in (1.21). To see this, note that (1.20), (I), and (4.6) (i.e., $\alpha \leq 0$) give $q \leq 0$. Therefore, the denominator in (4.8) satisfies $1 - \gamma + q < 0$, and (4.8) holds if and only if

$$\kappa(1 - \gamma + q) + 2\lambda(\sigma - 1) \leq 0.$$

Using (1.20) and (4.4) to substitute for q and σ , and rearranging, we obtain the equivalent condition

$$\frac{\alpha}{1+V_*} \leq \frac{n}{\kappa+n}[(\lambda-1) + \frac{\kappa}{2}(\gamma-1)] \equiv \frac{n\gamma\alpha}{\kappa+n}. \quad (4.9)$$

Recall that boundedness of $c(\bar{t}, r)$ near $r = 0$ requires (4.6), i.e., $\alpha \leq 0$. If $\alpha < 0$ (4.9) simplifies to

$$\frac{1}{1+V_*} \geq \frac{n\gamma}{\kappa+n},$$

which, according to (4.2), (I), and (1.16), reduces to

$$n(\gamma-1) \leq 2(\lambda-1). \quad (4.10)$$

However, $\alpha < 0$ also gives $2(\lambda-1) < -\kappa(\gamma-1)$, so that (4.10) yields $n(\gamma-1) < -\kappa(\gamma-1)$, or $n+\kappa < 0$. This contradicts the integrability condition (I), and we conclude that α must vanish, i.e., we must have $\kappa = \hat{\kappa}$. We observe that, with $\kappa = \hat{\kappa}$, (4.7) and (4.5) indeed provide bounded values for both $\rho(\bar{t}, r)$ and $c(\bar{t}, r)$ as $r \downarrow 0$. As detailed above (after (1.21)), it follows that the resulting flow in this case is globally isentropic. We sum up our findings in the following proposition:

Proposition 4.1. *Let $n = 2$ or 3 and fix $\gamma > 1$ and $\lambda > 0$. Consider any solution $(V(x), C(x))$ of the similarity ODEs (1.10)-(1.11), defined for $x < 0$ and satisfying (4.3) and (2.4) (with μ and ν finite and nonzero). Finally, let $R \geq 0$ be given by (1.19), and define the flow variables ρ, u, c according to (1.9).*

Then the requirements (I)-(III) in Section 4.1, together with boundedness of $\rho(t, r)$ and $c(t, r)$ as $r \downarrow 0$ at fixed times $t < 0$, imply that the similarity parameter κ in (1.9) must have the value $\hat{\kappa}$ given in (1.21). Finally, with $\kappa = \hat{\kappa}$ the resulting Euler flow (defined for $t < 0$) is necessarily isentropic.

From now on $\kappa = \hat{\kappa}$ is assumed. We note that the integrability conditions (I)-(III) in Section 4.1 then reduce to the single requirement (III), which now reads

$$\lambda < \bar{\lambda}(\gamma, n) := 1 + \frac{n}{2}(1 - \frac{1}{\gamma}). \quad (4.11)$$

This is trivially satisfied if $0 < \lambda < 1$, a fact we make use of in Section 5.

4.3. Isentropic behavior near $r = 0$. The arguments above show that with $\kappa = \hat{\kappa}$, any continuous solution of (1.10)-(1.11) which is defined for all $x < 0$ and satisfies (4.3) and (2.4), generates flow variables $u(\bar{t}, r)$, $c(\bar{t}, r)$, $\rho(\bar{t}, r)$ that approach finite values as $r \downarrow 0$ at each fixed $\bar{t} < 0$. We now verify that these finite values are approached with *bounded gradients*. In particular, no gradient catastrophe occurs in the flow prior to collapse at time $t = 0$.

First, consider $u_r(\bar{t}, r)$; according to (1.9) and (1.10) we have

$$u_r(\bar{t}, r) = -\frac{1}{\lambda t} \left(V(x) + \frac{G(V(x), C(x))}{D(V(x), C(x))} \right), \quad \text{where } x = \frac{\bar{t}}{r\lambda}.$$

Recalling that $C(x) \uparrow +\infty$ and $V(x) \rightarrow V_*$ as $r \downarrow 0$, we get from (1.14) that

$$\frac{G(V(x), C(x))}{D(V(x), C(x))} \rightarrow 0 \quad \text{as } r \downarrow 0.$$

It follows from this that

$$u_r(\bar{t}, r) \sim -\frac{V_*}{\lambda t} \quad \text{as } r \downarrow 0.$$

Similarly, using (1.9) and (1.11), we have

$$c_r(\bar{t}, r) = \frac{C(x)}{\lambda t} \left[\frac{(1-k_1)(1+V(x))^2 + k_2(1+V(x)) - k_3}{C(x)^2 - (1+V(x))^2} \right],$$

and it follows from (4.3) that $c_r(\bar{t}, r) \sim 0$ as $r \downarrow 0$. In particular, to leading order, $c(\bar{t}, r)$ is constant as $r \downarrow 0$. Finally, since $\rho \propto c^{\frac{2}{\gamma-1}}$ in isentropic flow, the same applies to the density field.

We conclude that, in the isentropic setting under consideration, at any fixed time $\bar{t} < 0$, all of $u_r(\bar{t}, r)$, $c_r(\bar{t}, r)$, $\rho_r(\bar{t}, r)$, and hence also $p_r(\bar{t}, r)$, remain bounded as $r \downarrow 0$. In particular, no gradient catastrophe occurs at $r = 0$ at strictly negative times.

On the other hand, at time of collapse $t = 0$, (2.4) and (1.9) give

$$\rho(0, r) = r^{\hat{\kappa}} R(0), \quad u(0, r) = -\frac{\nu}{\lambda} r^{1-\lambda}, \quad c(0, r) = -\frac{\omega}{\lambda} r^{1-\lambda}.$$

In particular, provided ν and ω are finite and nonzero, and $0 < \lambda < 1$, we see that both the velocity and sound speed suffer a gradient catastrophe at the origin at $t = 0$.

The same applies to the density field provided $\hat{\kappa} < 1$, i.e., $\lambda > \frac{3-\gamma}{2}$. Note that the latter inequality is satisfied whenever $\lambda > 0$ and $\gamma > 3$, as will be the case for the solutions we construct in Section 5. On the other hand, the pressure field at time of collapse is, by (1.5),

$$p(0, r) = \frac{1}{\gamma} \rho(0, r) c^2(0, r) \propto r^{\hat{\kappa}+2(1-\lambda)},$$

which suffers a gradient catastrophe at $r = 0$ provided $\hat{\kappa} + 2(1 - \lambda) < 1$, or equivalently,

$$\lambda > \frac{1}{2} \left(1 + \frac{1}{\gamma}\right). \quad (4.12)$$

As we shall see, (4.12) will be violated for all solutions we construct below: their pressure fields are at least C^1 -smooth at time of collapse.

Remark 4.2. We note that, with $\lambda \in (0, 1)$ and $\kappa := \hat{\kappa}$ the density field at time of collapse satisfies $\rho(0, r) \propto r^{\hat{\kappa}}$, which vanishes at the origin. The resulting Euler flow therefore has a one-point vacuum at the origin at time of collapse.

5. CONSTRUCTION OF CONTINUOUS FLOWS WITH $0 < \lambda < 1$ AND $\kappa = \hat{\kappa}$

We now turn to the construction of continuous, and in particular, locally bounded radial Euler flows with similarity variable $\lambda \in (0, 1)$. As explained in Section 4.2, we restrict attention to solutions satisfying (4.3), and Proposition 4.1 then shows that we must choose $\kappa = \hat{\kappa}$ in order to meet the physical constraints (I)-(III) in Section 4.1. Thus, for the remainder of the paper it is assumed that

$$0 < \lambda < 1 \quad \text{and} \quad \kappa = \hat{\kappa} = \frac{2(1-\lambda)}{\gamma-1}. \quad (5.1)$$

We observed at the end of Section 2.2.3 that $V_6 = V_-$ and $V_8 = V_+$ are both real under assumptions (5.1), so that the critical points P_1 - P_9 are all present.

5.1. Outline of construction. The continuous flows are built by identifying solution trajectories Γ_1 - Γ_3 of (1.10)-(1.11) with the properties

- (Π_1) Γ_1 connects $P_{+\infty}$ to P_8 ;
- (Π_2) Γ_2 connects P_8 to P_9 and passes through $P_1 = (0, 0)$;
- (Π_3) Γ_3 connects P_9 to $P_{-\infty}$.

The symmetries recorded in (2.2) effectively reduce our task to identifying only Γ_1 and Γ_2 : Γ_3 will simply be the reflection of Γ_1 about the V -axis, connecting P_9 to $P_{-\infty}$.

Recall from Section 2.3 that $P_{\pm\infty}$ are saddle points. In searching for a trajectory Γ_1 satisfying (Π_1) it is therefore advantageous that P_8 be a nodal point into which a large family of trajectories are drawn. Indeed, a key part of the following analysis (Section 5.4) concerns the identification of a (λ, γ) -regime for which P_8 is a proper node.

Care must be taken that Γ_1 reaches P_8 without crossing the critical line \mathcal{L}_+ . It turns out that the latter requirement fixes the spatial dimension to be $n = 3$ (see Section 5.4.2). Likewise, the trajectory Γ_2 must connect to the origin without crossing \mathcal{L}_+ ; this however, will not impose any further constraints on the parameters.

Having identified a suitable (λ, γ) -regime (for $n = 3$) we find it necessary to verify numerically that there are cases in which Γ_1 connects $P_{+\infty}$ to P_8 without first crossing \mathcal{L}_+ . With Γ_1 , and hence Γ_3 , thus determined, it remains to determine a suitable trajectory Γ_2 satisfying (Π_2). It is unproblematic to reach the origin P_1 from P_8 : among the trajectories leaving the node at P_8 , there are infinitely many that connect to the origin. However, as the trajectory is continued through the

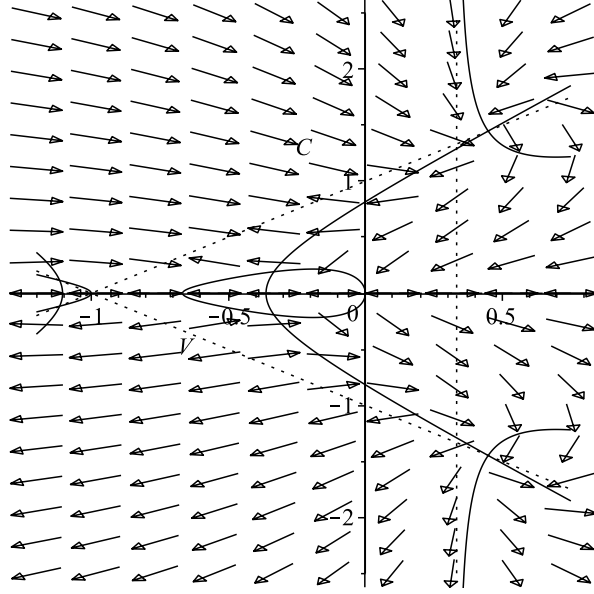


FIGURE 2. The direction field of (1.10)-(1.11), with $x < 0$ ($x > 0$) in the upper (lower) half-plane. The zero-levels of $F(V, C)$, $G(V, C)$, the critical lines $\mathcal{L}_{\pm} = \{C = \pm(1 + V)\}$, and the axes are solid curves; the vertical asymptote $V = V_*$ is dotted. The parameters are as in Figure 1: $n = 3$, $\gamma = \frac{5}{3}$, $\lambda = \frac{2}{3}$, and $\kappa = \hat{\kappa} = 1$.

origin, it should subsequently be drawn into P_9 . It turns out that this last requirement determines a range of possible slopes with which Γ_2 can reach P_1 ; see Section 5.5. Again, we verify numerically the existence of trajectories Γ_2 meeting these constraints.

We note that it is necessary to make a final check on the selected trajectories Γ_1 - Γ_3 : they must provide admissible solutions trajectories for the original ODE system (1.10)-(1.11) (as opposed to the single ODE (1.12)). As explained in Section 2.1, any solution $(V(x), C(x))$ of physical relevance must necessarily pass through the origin P_1 with $x = 0$, and from the upper half-plane to the lower half-plane as x increases. Also, they must move along Π_1 - Π_2 - Π_3 in the correct direction given by (1.10)-(1.11) as x increases from $-\infty$ to $+\infty$.

Figure 2 provides a representative case of the vector field $(-\frac{1}{\lambda x} \frac{G(V, C)}{D(V, C)}, -\frac{1}{\lambda x} \frac{F(V, C)}{D(V, C)})$ corresponding to the ODE system (1.10)-(1.11), with $x < 0$ ($x > 0$) in the upper (lower) half-plane. Notice that the arrows provide the actual direction of flow for solutions $(V(x), C(x))$ as x increases.

Remark 5.1. Figure 2 illustrates the impossibility of having a solution of the ODE system (1.10)-(1.11) cross the critical lines $\mathcal{L}_{\pm} = \{C = \pm(1 + V)\}$ at a non-singular point: such trajectories of the autonomous ODE (1.12) fail to yield relevant solutions to (1.10)-(1.11) since the vector field corresponding to (1.10)-(1.11) points in opposite directions on either side of \mathcal{L}_{\pm} .

Note that the parameters in Figure 2 are chosen for illustrative purposes; in particular, the behavior near P_8 is such that property (Π_1) fails in this case. It will be shown below that to satisfy (Π_1) , we need to choose $n = 3$, λ sufficiently small, and γ sufficiently large. It turns out that with such parameter values it is necessary to zoom in at the critical points P_8 , P_1 , and P_9 in order to display the behavior there; see Figures 6 and 7.

5.2. Location of critical points. We start by determining the relative V -locations of the critical points under the assumptions in (5.1). For convenience we repeat the expressions for V_{\pm} (see (2.16)

and (2.17)) and V_* in terms of $\mu = \lambda - 1$:

$$V_{\pm} = \frac{1}{2}(a \pm \sqrt{Q}) \quad \text{and} \quad V_* = \frac{-2\mu}{n(\gamma-1)}, \quad (5.2)$$

where

$$a = \frac{(\gamma-3)}{m(\gamma-1)}\mu - 1 \quad Q = \left(\frac{(\gamma-3)}{m(\gamma-1)}\right)^2 \mu^2 - 2\frac{(\gamma+1)}{m(\gamma-1)}\mu + 1. \quad (5.3)$$

Recalling (2.6) and introducing the positive constant

$$k := \frac{m}{2}[n(\gamma-1) + 2], \quad (5.4)$$

we have

$$V_4 = -\frac{m}{k}(1 + \mu). \quad (5.5)$$

For later reference we note that

$$V_8 - V_6 \equiv V_+ - V_- = \sqrt{Q}, \quad (5.6)$$

and

$$V_8 - V_4 = \frac{1}{2} \left[\left(\frac{(\gamma-3)}{m(\gamma-1)} + \frac{2m}{k} \right) \mu + \left(\frac{2m}{k} - 1 \right) + \sqrt{Q} \right] \quad (5.7)$$

Lemma 5.1. *Assuming $n = 2$ or 3 , $\gamma > 1$, and that (5.1) holds, we have*

$$V_6 < V_2 = -1 < V_3 = -\lambda < V_4 < 0 < V_* < V_8. \quad (5.8)$$

Proof. We consider each inequality in turn, from left to right:

- $V_6 = V_- < -1$: According to (5.2)₁ this inequality amounts to

$$a + 2 < \sqrt{Q}. \quad (5.9)$$

It is immediate to verify that $a + 2 > 0$ if and only if $(\gamma - 1)(\mu + m) > 2\mu$, which holds since $m \geq 1$, $-1 < \mu < 0$, and $\gamma > 1$. It follows that (5.9) is equivalent to $(a + 2)^2 < Q$; substituting from (5.3) shows that the latter inequality reduces to $\gamma > 1$, establishing the first inequality.

- $-1 < -\lambda$: Immediate by (5.1)₁.
- $-\lambda < V_4$: Substituting from (5.4) and (5.5), and recalling that $\mu + 1 = \lambda > 0$, this inequality reduces to $n(\gamma - 1) > 0$, which holds since $\gamma > 1$.
- $V_4 < 0$: Immediate from (5.5) since m, k (see (5.4)), and $\mu + 1 = \lambda$ are all positive.
- $0 < V_*$: Immediate from (5.2)₂ since $\mu < 0 < \gamma - 1$.
- $V_* < V_8 = V_+$: By substituting from (5.2) we obtain the equivalent inequality

$$-\frac{4\mu}{n(\gamma-1)} - a < \sqrt{Q}. \quad (5.10)$$

Using the expression for a in (5.3) and rearranging, we get that the left-hand side of (5.10) is positive provided $n(\gamma + 1) - 4 > \frac{mn(\gamma-1)}{\mu}$, which holds since the left-hand side in the latter inequality is positive (because $n \geq 2$ and $\gamma > 1$), while the right-hand side is negative. It follows that (5.10) is equivalent to

$$\left(\frac{4\mu}{n(\gamma-1)} + a \right)^2 < Q. \quad (5.11)$$

Substituting from (5.3) for a and Q , and simplifying the result, we obtain that (5.11) is equivalent to $n(\gamma - 1) > -\mu(n(\gamma - 1) - 1)$, which holds since $\gamma > 1$ and $-\mu = 1 - \lambda < 1$. \square

5.3. The critical point $P_{+\infty}$. This analysis was done in Section 2.3, and it was noted there that $P_{+\infty} = (V_*, +\infty)$ is necessarily a saddle point when $\kappa = \hat{\kappa}$. It follows that there is a unique trajectory Γ_1 of (1.12) which approaches $P_{+\infty}$. An inspection of $F(V, C)$ and $G(V, C)$ shows that the solutions of (1.12) have negative slopes within the the region

$$\Omega := \{(V, C) \mid V_* < V < V_8, 1 + V < C < \bar{C}(V)\} \quad (5.12)$$

where $C = \bar{C}(V)$ denotes the V -parametrization of the zero-level \mathcal{G} of G . Furthermore, their slopes are finite along $V = V_*$ and infinite along $C = \bar{C}(V)$. It follows that Γ_1 is located within Ω and can reach its boundary only along $C = 1 + V$ for some $V \in (V_*, V_8)$, or at P_8 . In order to be useful for our purpose of building a globally defined fluid flow, we must have that Γ_1 passes through P_8 . We proceed to analyze the behavior of (1.12) around P_8 .

5.4. Behavior near P_8 ; construction of Γ_1 . In this subsection, unless indicated differently, all quantities are evaluated at $P_8 = (V_8, C_8)$, and the subscript ‘8’ is suppressed in most of the expressions. To determine the type of the critical point P_8 we shall need the signs of various quantities given in terms of the partial derivatives of F and G there. First, since $P_8 \in \mathcal{L}_+ \cap \mathcal{F} \cap \mathcal{G}$ we have

$$C = 1 + V \quad (5.13)$$

$$C^2 = k_1(1 + V)^2 - k_2(1 + V) + k_3 \quad (5.14)$$

$$C^2 = \frac{V(1+V)(\lambda+V)}{n(V-V_*)}. \quad (5.15)$$

At P_8 we then have

$$F_C = 2C^2 \quad (5.16)$$

$$F_V = C(k_2 - 2k_1(1 + V)) \quad (5.17)$$

$$G_C = 2nC(V - V_*) \equiv 2V(\lambda + V) \quad (5.18)$$

$$G_V = C(n - \lambda + nV_* - 2V). \quad (5.19)$$

Here, F_C and F_V are calculated from (1.15) (using that $\alpha = 0$ when $\kappa = \hat{\kappa}$), while G_C and G_V are calculated from (1.14), and using that

$$nC(V - V_*) = V(\lambda + V),$$

the latter being a consequence of (5.13) and (5.15). We note that (5.16), (5.18), and (5.19) give

$$F_C > 0 \quad \text{and} \quad G_C > 0. \quad (5.20)$$

Next, using the expressions above, we obtain that

$$G_V + G_C = C(2mV + m - \mu - nV_*), \quad (5.21)$$

and substitution of the expressions in (5.2) for $V = V_8 = V_+$ and V_* then yields

$$G_V + G_C = mC\sqrt{Q} > 0. \quad (5.22)$$

Applying (2.1), we therefore obtain

$$F_V + F_C = -\frac{(\gamma-1)}{2}(G_V + G_C) < 0, \quad (5.23)$$

so that

$$F_V < -F_C < 0. \quad (5.24)$$

Finally, we note that the expressions above give

$$F_C + G_V = C \left(n + 1 - \frac{\gamma+1}{\gamma-1}\mu \right) > 0. \quad (5.25)$$

We next recall some notation and results from Lazarus [17]. The Wronskian is defined by

$$W := F_C G_V - F_V G_C,$$

and the discriminant by

$$R^2 := (F_C - G_V)^2 + 4F_V G_C \equiv (F_C + G_V)^2 - 4W. \quad (5.26)$$

In the following, whenever $R^2 > 0$, we set $R := +\sqrt{R^2} > 0$. Next, with

$$L_{1,2} = \frac{1}{2G_C}(F_C - G_V \pm R) \quad (5.27)$$

and

$$E_{1,2} = \frac{1}{2G_C}(F_C + G_V \pm R), \quad (5.28)$$

and signs chosen so that

$$|E_1| < |E_2|, \quad (5.29)$$

we have that integrals of (1.12) near P_8 approach one of the curves

$$(c - L_1 v)^{E_1} = \text{constant} \times (c - L_2 v)^{E_2},$$

where $v = V - V_8$ and $c = C - C_8$. Note that the signs \pm in (5.27) and in (5.28) agree; L_1 and L_2 are referred to as the *primary* and *secondary* slopes (or directions), respectively. Provided that $R^2 > 0$ (so that R is real and positive) and $W > 0$, P_8 is a proper node. In this case all solution curves approaching P_8 do so with slope equal to the primary slope L_1 , except one which approaches P_8 with slope L_2 .

An elegant argument by Lazarus [17] shows that $W \equiv W_8$ is given as

$$W = 2kC_8^2(V_8 - V_4)(V_8 - V_6), \quad (5.30)$$

where $k > 0$ is given in (5.4). It follows from Lemma 5.1 that

$$W > 0. \quad (5.31)$$

We now assume that $R^2 > 0$ (this requirement is addressed below in Section 5.4.1) and proceed to determine the signs to be used in (5.27) so that (5.29) is satisfied. According to (5.28), (5.29) holds if and only if

$$|F_C + G_V \pm R| < |F_C + G_V \mp R|. \quad (5.32)$$

From (5.25) we have that $F_C + G_V > 0$, and since $W > 0$ we have

$$0 < R = \sqrt{(F_C + G_V)^2 - 4W} < F_C + G_V. \quad (5.33)$$

It follows that the minus-sign should be used on the left hand side of (5.32), and the plus-sign should be used on the right hand side of (5.32). That is, under the condition that $R^2 > 0$, together with the standing assumption (5.1), we have

$$L_1 = \frac{1}{2G_C}(F_C - G_V - R) \quad \text{and} \quad L_2 = \frac{1}{2G_C}(F_C - G_V + R). \quad (5.34)$$

With this we have that P_8 is a proper node and that all but one of the integrals of (1.12) approaching P_8 do so with slope L_1 .

We next want to determine how the primary slope L_1 compares to those of the curves \mathcal{G} and \mathcal{L}_+ at P_8 . Let $\bar{C}(V)$ be the V -parametrization of the zero-level curve \mathcal{G} for $G(V, C)$, so that $\bar{C}'(V_8) = -\frac{G_V}{G_C}$. Together with (5.34)₁, and the fact that $G_C > 0$ (by (5.20)₂), this implies that the inequality $L_1 > \bar{C}'(V_8)$ is equivalent to $F_C + G_V > R$, which holds according to (5.33). Therefore, near P_8 , the straight line

$$\mathcal{L}_1 : \quad C = C_8 + L_1(V - V_8)$$

is located below \mathcal{G} for $V < V_8$ and above \mathcal{G} for $V > V_8$.

Before proceeding we also note the following: with $\tilde{C}(V)$ denoting the V -parametrization of the zero-level curve \mathcal{F} for $F(V, C)$, we have $\tilde{C}'(V) = -\frac{F_V}{F_C}$, and it follows from (5.20)₁ and (5.23) that $\tilde{C}'(V_8) > 1$. Similarly, using (5.20)₂ and (5.22), we have $\tilde{C}'(V_8) < 1$.

Finally, since $\frac{dC}{dV} = \frac{F}{G} < 0$ within the region Ω given in (5.12), a *necessary* condition for having Γ_1 approach P_8 is that $L_1 < 0$. As $G_C > 0$, (5.34)₁ shows that this condition amounts to

$$F_C < R + G_V. \quad (5.35)$$

Our goal now is to identify a parameter regime $(\lambda, \gamma) \in (0, 1) \times (1, \infty)$ for which both of the two requirements $R^2 > 0$ and $L_1 < 0$ are satisfied. As demonstrated below in Lemma 5.3, this requires $n = 3$, $0 < \lambda < \frac{1}{9}$, and γ sufficiently large. For such parameter values we then verify numerically that there are cases in which

- there are integrals of (1.12) passing through the node P_8 along the primary direction L_1 and crossing the vertical line $V = V_*$; and
- there are other integrals of (1.12) passing through the node P_8 along the primary direction L_1 and crossing \mathcal{G} vertically.

It then follows by continuity that the unique integral Γ_1 of (1.12) which approaches the critical point $P_{+\infty} = (V_*, +\infty)$, also passes through P_8 along the primary direction L_1 .

5.4.1. *The requirement $R^2(\lambda, \gamma) > 0$.* The discriminant R^2 is given in (5.26); fixing $n = 2$ or 3 , it is a function $R^2(\lambda, \gamma)$. According to (5.25), (5.26), and (5.30), we have $R^2(\lambda, \gamma) > 0$ if and only if

$$\left(n + 1 - \frac{\gamma+1}{\gamma-1}\mu\right)^2 > 8k(V_8 - V_4)(V_8 - V_6). \quad (5.36)$$

For each choice of $n = 2$ or 3 this inequality defines a certain region in the (λ, γ) -plane, which, according to our standing assumption (5.1)₁, is located within the half-strip $\{0 < \lambda < 1, \gamma > 1\}$. As the next lemma shows, the location of this region depends sensitively on n .

Lemma 5.2. *For $\lambda \in (0, 1)$ fixed, we have*

$$\lim_{\gamma \uparrow +\infty} R^2(\lambda, \gamma) > 0 \quad \Longleftrightarrow \quad \begin{cases} \lambda \in (0, \frac{1}{9}) & \text{when } n = 3 \\ \lambda \in (\frac{8}{9}, 1) & \text{when } n = 2. \end{cases}$$

Proof. Sending $\gamma \uparrow \infty$ in the expressions in (5.3), we get

$$a \rightarrow a_\infty := \frac{\mu}{m} - 1 < 0, \quad Q \rightarrow Q_\infty := a_\infty^2.$$

It follows from (5.2) that $V_8 = V_+ \rightarrow \frac{1}{2}(a_\infty + |a_\infty|) = 0$, and $V_6 = V_- \rightarrow \frac{1}{2}(a_\infty - |a_\infty|) = a_\infty$. Also, from (5.4) and (2.6) we have that $V_4 \rightarrow 0$, while $kV_4 = -m(1 + \mu)$. As $\gamma \uparrow \infty$ the requirement $R^2 > 0$ in (5.36) therefore reduces to the condition

$$(n + 1 - \mu)^2 > 8|a_\infty| \left[\lim_{\gamma \uparrow \infty} k(V_8 - V_4) \right] = 8(1 - \frac{\mu}{m}) \left[m(1 + \mu) + \lim_{\gamma \uparrow \infty} kV_8 \right], \quad (5.37)$$

where the last limit is of the form “ $\infty \cdot 0$.” To analyze it we determine more precisely the distance between Q and Q_∞ , and between a and a_∞ , as $\gamma \uparrow \infty$. Rewriting the expression (5.3)₂ for Q , we find that

$$Q = (1 - \frac{\mu}{m})^2 - \frac{4\mu}{m(\gamma-1)} \left[1 + \frac{\mu}{m} \left(\frac{\gamma-2}{\gamma-1} \right) \right] \sim (1 - \frac{\mu}{m})^2 - \frac{4\mu(m+\mu)}{m^2(\gamma-1)} \quad \text{as } \gamma \uparrow \infty.$$

To leading order in γ we therefore have

$$\sqrt{Q} \sim (1 - \frac{\mu}{m}) - \frac{2\mu(m+\mu)}{m(m-\mu)} \frac{1}{(\gamma-1)} \quad \text{as } \gamma \uparrow \infty.$$

Combining this with

$$a = (\frac{\mu}{m} - 1) - \frac{2\mu}{m} \frac{1}{(\gamma-1)},$$

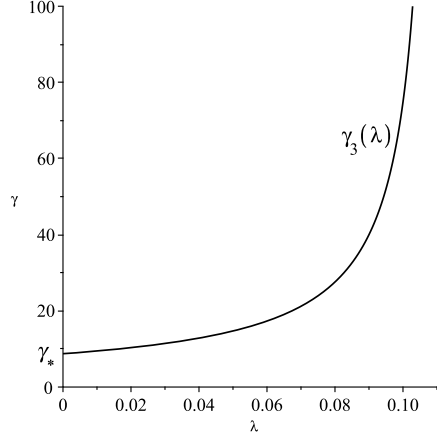


FIGURE 3. The graph of the function $\gamma_3(\lambda)$ which is defined for $0 < \lambda < \frac{1}{9}$; the discriminant $R^2(\lambda, \gamma)$ in (5.26) is positive when $\gamma > \gamma_3(\lambda)$; $\gamma_* = \gamma_3(0) \approx 8.72$.

gives

$$V_8 = \frac{1}{2}(a + \sqrt{Q}) \sim -\frac{2\mu}{(m-\mu)} \frac{1}{(\gamma-1)} \quad \text{as } \gamma \uparrow \infty.$$

Recalling the expression (5.4) for k we obtain

$$\lim_{\gamma \uparrow \infty} kV_8 = -\frac{mn\mu}{m-\mu}.$$

Using this in (5.37) we conclude that, as $\gamma \uparrow \infty$, the requirement $R^2 > 0$ reduces to the condition

$$(n+1-\mu)^2 > 8[(m-\mu)(1+\mu) - n\mu]. \quad (5.38)$$

Finally, with $n = 3$ ($m = 2$), (5.38) becomes $8\mu + 9\mu^2 > 0$, which reduces to $\lambda = 1 + \mu < \frac{1}{9}$; with $n = 2$ ($m = 1$), (5.38) becomes $(1+\mu)(1+9\mu) > 0$, which reduces to $\lambda > \frac{8}{9}$. \square

Numerical plots of the curve in the (λ, γ) -plane defined by $R^2(\lambda, \gamma) = 0$ reveal that it is the graph of an:

- increasing function $\lambda \mapsto \gamma_3(\lambda)$ defined for $\lambda \in (0, \frac{1}{9})$ and with a vertical asymptote at $\lambda = \frac{1}{9}$ when $n = 3$;
- decreasing function $\lambda \mapsto \gamma_2(\lambda)$ defined for $\lambda \in (\frac{8}{9}, 1)$ and with a vertical asymptote at $\lambda = \frac{8}{9}$ when $n = 2$.

Figure 3 shows the situation for $n = 3$; the minimum value of $\gamma_3(\lambda)$ is $\gamma_* := \gamma_3(0) \approx 8.72$.

5.4.2. The requirement $L_1 < 0$. For n fixed we now consider R^2 and L_1 as functions of λ and γ . Recall that $L_1(\lambda, \gamma) < 0$ is a necessary condition for having the trajectory Γ_1 connect $P_{+\infty}$ to P_8 , and that we want P_8 to be a node, i.e., we need $R^2(\lambda, \gamma) > 0$. The following lemma shows that only the case $n = 3$ is favorable in this regard.

Lemma 5.3. *For $\lambda \in (0, 1)$ and $\gamma > 1$ we have*

- (1) *for $n = 3$: if $R^2(\lambda, \gamma) > 0$, then $L_1(\lambda, \gamma) < 0$;*
- (2) *for $n = 2$: if $R^2(\lambda, \gamma) > 0$, then $L_1(\lambda, \gamma) > 0$.*

Proof. As detailed above, the requirement $L_1 < 0$ amounts to the inequality in (5.35). First, if $n = 3$ and $R^2 > 0$ (so that $R > 0$), then (5.35) follows once we verify that $F_C < G_V$. A direct calculation shows that the latter inequality (for $n = 3$) reduces to

$$4(\gamma - 3)(\gamma - 1) > \mu(3\gamma - 5)(\gamma + 1),$$

which is trivially satisfied whenever $\gamma > 3$ since $\mu = \lambda - 1 < 0$. According to the analysis above, $R^2 > 0$ implies $\gamma > \gamma_* > 3$ when $n = 3$, establishing part (1) of the lemma.

Next consider the case $n = 2$. According to (5.34) and (5.20), the inequality $L_1 > 0$ amounts to $F_C - G_V > R$. For $n = 2$ it follows from (5.16), (5.19), and (5.13), that $F_C > G_V$ if and only if

$$2V_8 + \frac{\lambda}{2} > V_*,$$

which is satisfied since $\lambda > 0$ and $V_8 > V_*$ (by Lemma 5.1). If $R^2 > 0$, so that $R > 0$, it follows that $F_C - G_V > R$ holds if and only if $(F_C - G_V)^2 > R^2$. Substituting from (5.26) for R^2 shows that the latter inequality reduces to $F_V G_C < 0$, which is satisfied according to (5.20)₂ and (5.24). We conclude that, for $n = 2$, $L_1 > 0$ whenever $R^2 > 0$. \square

With this we have identified the relevant parameter regime in which to search for continuous similarity flows when $\lambda \in (0, 1)$: we need to choose $n = 3$, and (λ, γ) so that $R^2(\lambda, \gamma) > 0$, i.e., $\lambda \in (0, \frac{1}{9})$ and $\gamma > \gamma_3(\lambda)$. This guarantees that P_8 is a node with a negative primary slope L_1 . It remains to provide examples in which the trajectory Γ_1 from $P_{+\infty}$ is drawn into P_8 . As noted above, a sufficient condition for this behavior is the existence of trajectories that enter the region Ω (see (5.12)) along its left edge at $V = V_*$, and from there continue on to reach P_8 . The numerical verification of this condition is addressed in Section 5.7.

Before moving on to the behavior near P_1 we note the following consequence of the proof of Lemma 5.3: when $n = 3$ and $R^2(\lambda, \gamma) > 0$, then $L_1(\lambda, \gamma) < L_2(\lambda, \gamma) < 0$. Indeed, $L_1(\lambda, \gamma) < L_2(\lambda, \gamma)$ holds by definition, while the inequality $L_2(\lambda, \gamma) < 0$ amounts to $R < G_V - F_C$. The proof of Lemma 5.3 showed that when $n = 3$ and $R^2(\lambda, \gamma) > 0$, then $G_V - F_C > 0$. Therefore, $R < G_V - F_C$ holds provided $R^2 < (G_V - F_C)^2$, which, according to (5.26), amounts to $F_V G_C < 0$. The latter inequality is satisfied according to (5.20)₂ and (5.24).

5.5. Behavior near P_1 ; construction of Γ_2 . While there is (at most) a single trajectory Γ_1 joining $P_{+\infty}$ to P_8 , there will be a continuum of trajectories joining P_8 to P_9 via the proper node P_1 at the origin. To identify these it is convenient to also classify the critical point P_4 . Lazarus [17] shows that the the Wronskian there is given as

$$W_4 = 2kC_4^2(V_4 - V_6)(V_4 - V_8), \quad (5.39)$$

where k is a positive constant (cf. (5.30)). It follows from Lemma 5.1 that $W_4 < 0$ so that P_4 , and hence also P_5 , are saddle points. An inspection of the (V, C) -plane reveals the presence of three relevant separatrices (see Figure 6):

- Θ joining P_8 to P_4 ;
- Φ joining P_4 to P_1 ; and
- Ψ joining P_1 to P_5 .

Let $\zeta > 0$ denote the slope of Ψ at P_1 ; by symmetry, the slope of Φ at P_1 is then $-\zeta$.

The trajectories Γ_2 of interest to us (i.e., the ones leading to continuous Euler flows) are those that reach the origin P_1 from P_8 , and then moves on to P_9 in the lower half-plane.

As is clear from Figure 6, in order for Γ_2 to reach the origin, it must be located to the right of the separatrix Θ . Also, it follows from the analysis at the end of Section 5.4.2 that all trajectories leaving P_8 do so with a negative slope: either L_1 or L_2 , where $L_1 < L_2 < 0$. Let Γ_s denote the unique one among these which leaves with slope L_2 .³ Now, all trajectories leaving P_8 (with $V(x)$ increasing) proceed to cross vertically that part of the zero-level $\mathcal{G} = \{G = 0\}$ which is located in the first quadrant. Among these, some reach the origin with negative slopes after having vertically crossed also that part of \mathcal{G} located in the second quadrant within the half-strip

³If we use the trajectory Γ_s the resulting Euler flow will suffer a *weak* discontinuity (i.e., a discontinuity in the first derivatives of the flow variables) across a curve $r(t) = (\frac{t}{x_8})^{\frac{1}{\lambda}}$ in the (r, t) -plane, where $x_8 < 0$ is such that $(V(x_8), C(x_8)) = P_8$. This curve is a 1-characteristic for the radial Euler system (1.6)-(1.8).

$\{(V, C) : V_4 < V < 0, C > 0\}$. In all cases we have considered, it is clear from numerical tests that there are other trajectories from P_8 which reach P_1 with positive slopes; see Remark 5.2 below. In the following discussion it is assumed that this is the case. Evidently, the smallest positive slope with which P_1 can be reached from P_8 is that with which Γ_s approaches P_1 ; we denote the latter slope by $\epsilon > 0$.

We next observe that the trajectory Γ_2 is not allowed to change its slope as it passes through P_1 .⁴ Recalling the symmetry (2.2) of the phase portrait, and setting $\delta := \max(\zeta, \epsilon) > 0$, we have that any of the infinitely many trajectories from P_8 which arrives at P_1 with a slope $s \in (-\infty, -\delta) \cup (\delta, +\infty]$, continues into the lower half-plane and reaches P_9 . Indeed, the part of its trajectory in the lower half-plane will simply be the reflection about the V -axis of one of the other trajectories from P_8 to P_1 , viz. the one arriving at P_1 with slope $-s$. (In the limiting case that Γ_2 reaches P_1 vertically, the lower part of Γ_2 is simply the reflection of its upper part about the V -axis.) Any one of these trajectories may serve as Γ_2 in our construction of continuous Euler flows.

Remark 5.2. *If Γ_s reached P_1 with slope $\epsilon < 0$, then none of the trajectories reaching the origin P_1 from P_8 would reach P_9 . Again, we have not observed this scenario in any of our numerical tests. E.g., in the case displayed in Figures 5 and 6 (with $n = 3$, $\lambda = 0.02$, $\gamma = 12$), ϵ is positive but so small that Γ_s is indistinguishable from the V -axis near the origin.*

5.6. Summary. We briefly summarize our findings so far in this section. First, by imposing the conditions $W > 0$ and $R^2 > 0$ at the critical point P_8 , we guarantee that P_8 is a node. The former requirement is automatically met once (5.1) holds, while the second requirement puts an n -dependent constraint on λ and γ . The further condition $L_1(\lambda, \gamma) < 0$, which is necessary in order that the trajectory Γ_1 connects to P_8 without first crossing \mathcal{L}_+ , implies that the space dimension n must be 3. With $n = 3$, the requirement $R^2 > 0$ is met, provided (λ, γ) lies above a certain graph $\gamma_3(\lambda)$ defined for $0 < \lambda < \frac{1}{9}$. If this is the case, then $L_1(\lambda, \gamma) < 0$ is automatically satisfied.

Next, for all cases we have investigated numerically (see Section 5.7), there is an infinite number of trajectories Γ_2 joining P_8 to P_9 and passing through the origin P_1 . Care must be taken that the trajectory from P_8 arrives at P_1 with a slope s for which another trajectory arrives at P_1 from P_8 with the slope $-s$. When this holds, Γ_2 consists of the former trajectory together with the reflection of the latter about the V -axis.

Finally, the trajectory Γ_3 joining P_9 to $P_{-\infty}$ is the reflection of Γ_1 about the V -axis.

To finish the argument for the existence of continuous, radial similarity Euler flows, as described in the Main Results, it remains to verify the following two points:

- (i) with $n = 3$, there are choices of $\lambda \in (0, \frac{1}{9})$ and $\gamma > \gamma_3(\lambda)$ such that the trajectory Γ_1 from $P_{+\infty}$ reaches P_8 , and
- (ii) for these choices of the parameters there are trajectories Γ_2 from P_8 reaching the origin and with the following property: Γ_2 reaches the origin with slope s , where $|s| > \delta$ (δ defined as above), and there is another trajectory from P_8 reaching the origin with slope $-s$.

Below we describe the numerical verification of these points.

5.7. Numerical verification of (i) and (ii). The numerical verification is carried out with Maple. As explained in Sections 5.3 and 5.4, to verify (i) it suffices to show that there is at least one solution crossing into the region Ω (see (5.12)) along $V = V_*$ and reaching P_8 without first crossing the critical line \mathcal{L}_+ . To numerically check this, it is convenient to switch to the variables $W := V - V_*$ and $Z := C^{-2}$ which were used in Section 2.3 to analyze the critical point $P_{+\infty}$. The latter point is then located at the origin of the (W, Z) -plane. The analysis in Section 2.3 shows

⁴This points out a difference between P_1 and the critical points P_6 - P_9 . As noted above, a change of slope as $(V(x), C(x))$ passes through P_8 , say, results in a weak discontinuity in the corresponding Euler flow. In contrast, a change in slope at P_1 would generate, via (1.9) and (2.4), an un-physical jump discontinuity across $t = 0$.

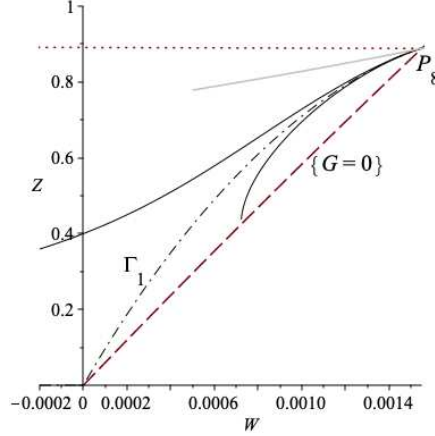


FIGURE 4. The dash-dot curve is an approximation of the trajectory Γ_1 when plotted in the (W, Z) -plane, where $W = V - V_*$ and $Z = C^{-2}$. The dashed curve is the zero-level $\mathcal{G} = \{G = 0\}$ (crossed vertically by trajectories), and the dotted curve is the critical line \mathcal{L}_+ . The two solid curves are solutions: the upper one passes through the point $(W, Z) = (0, 0.3)$ while the lower one starts out near \mathcal{G} . Finally, the grey curve indicates the primary slope with which the solutions reach P_8 . The parameter values are $n = 3$, $\lambda = 0.02$, and $\gamma = 12$. Evidently, Γ_1 reaches P_8 without first crossing \mathcal{L}_+ ; this is confirmed by further numerical plots near P_8 .

that this is a saddle point and that Γ_1 leaves $P_{+\infty} = (0, 0)$ with slope $\frac{dZ}{dW} = \frac{n+2}{B} = \frac{5}{B}$, where B is given in (2.21). A sufficient condition for (i) to hold is that there are trajectories through points on the positive Z -axis which reach P_8 without first crossing \mathcal{L}_+ .

Figure 4 displays the situation in the (W, Z) -plane for $n = 3$, $\lambda = 0.02$, and $\gamma = 12$, and provides clear numerical evidence that this is indeed the case. (The approximation of Γ_1 , the dash-dot curve in Figure 4, is obtained by starting very close to the origin along the straight line $Z = \frac{5}{B}W$.)

For numerical verification of (ii) we return to the (V, C) -plane and compute various trajectories joining the node at P_8 to the proper node (star point) P_1 at the origin. Figures 5 and 6 display the situation for the same parameter values as in Figure 4. Figure 5 shows the trajectory Γ_s leaving P_8 along the secondary direction and reaching the origin with a very small slope $\epsilon > 0$. It also shows a complete Γ_2 -trajectory, joining P_8 to P_9 via the origin, which appears to be symmetric about the V -axis. However, it is slightly un-symmetric and obscures the presence of the P_4P_8 -separatrix Θ ; see Figure 6 for the detailed situation near the origin.

5.8. The flow at collapse and absence of shocks. Figures 5-6 display a continuous trajectory Γ_2 joining the critical points P_8 and P_9 via the critical point P_1 at the origin. When this is joined with the trajectories Γ_1 and Γ_3 (the latter being the reflection of Γ_1 about the V -axis), we obtain a global, continuous solution $(V(x), C(x))$ of (1.10)-(1.11) joining $P_{+\infty}$ to $P_{-\infty}$ as x varies from $-\infty$ to $+\infty$. Finally, from this we obtain, according to (1.9), a globally defined, *continuous*, radial similarity Euler flow.

We now observe that whenever Γ_2 is a trajectory joining P_8 and P_9 via the origin, the same is true for its reflection Γ'_2 about the V -axis. Assuming Γ_2 reaches the origin with negative slope (as in Figures 5-6), the trajectory Γ'_2 will have positive slope at the origin. We therefore obtain two, physically distinct, Euler flows from these trajectories. In particular, since both Γ_2 and Γ'_2 reach the origin as $x \uparrow 0$, but with opposite signs of $V(x)$, the corresponding Euler flows display different

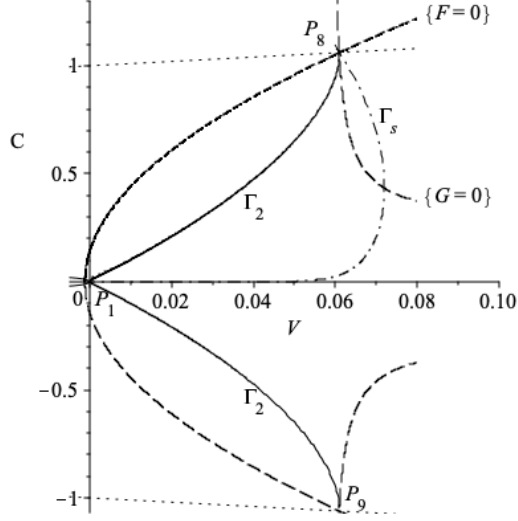


FIGURE 5. The dashed curves are the zero-levels $\{F = 0\}$ and $\{G = 0\}$, and the dash-dot curve the Γ_s -trajectory which leaves P_8 along the secondary direction. In addition there are two more solution trajectories: one is the separatrix Θ joining P_4 to P_8 , and the other is a complete Γ_2 -trajectory (solid curve) joining P_8 and P_9 via the origin P_1 . However, at this resolution the latter two trajectories are indistinguishable, and the Γ_2 trajectory appears symmetric about the V -axis. (Figure 6 displays a zoom-in near the origin which shows that this is not actually so.) The parameter values are as in Figure 4: $n = 3$, $\lambda = 0.02$, and $\gamma = 12$.

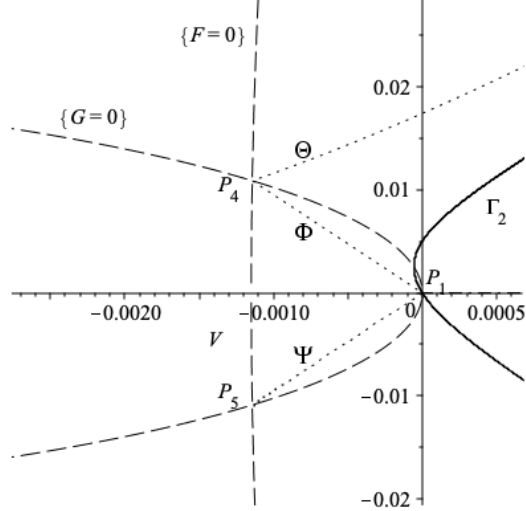


FIGURE 6. Zoom-in near the origin of Figure 5. The dashed curves are the zero-levels $\{F = 0\}$ and $\{G = 0\}$ the dotted curves are the separatrices Θ , Φ , and Ψ , and the solid curve is the Γ_2 -trajectory joining P_8 and P_9 via the origin P_1 . Note that the Γ_s -trajectory is indistinguishable from the V -axis near the origin; thus $\epsilon \gtrsim 0$ and $\delta = \zeta$ in this case.

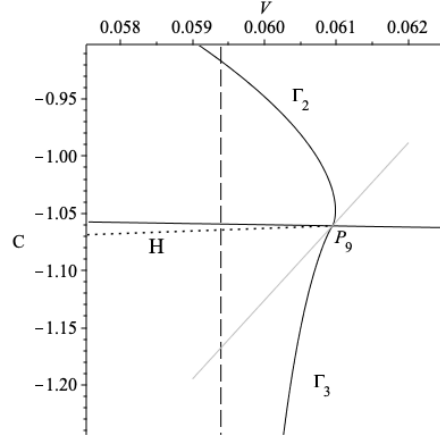


FIGURE 7. Zoom-in near the critical point P_9 with the same parameter values as in Figures 4-6: $n = 3$, $\lambda = 0.02$, and $\gamma = 12$. The solid straight line is the critical line $\mathcal{L}_- = \{C = -1 - V\}$, which appears almost horizontal. The solid trajectory consists of parts of Γ_2 and Γ_3 , located above and below \mathcal{L}_- , respectively; these meet at P_9 along the primary direction (grey line). The dashed vertical line is the asymptote $V = V_*$ approached by Γ_3 . Finally, the dotted curve is the Hugoniot locus H consisting of states to which points along Γ_2 can jump. Note that H is located below \mathcal{L}_- (as dictated by the entropy condition), but does not intersect Γ_3 before reaching P_9 . As a consequence, no shock wave occurs in the corresponding Euler flow subsequent to collapse.

behaviors at time of collapse: in the one built from Γ_2 the fluid is moving toward the origin at time of collapse, while in the one built from Γ'_2 it moves outward.

We find it noteworthy that the former flow remains continuous beyond collapse. The flow variables $\rho(0, r)$, $u(0, r)$, $c(0, r)$ all suffer gradient blowup at $r = 0$ (see Section 4.3), and in addition the fluid flow is directed inward. It would be reasonable to expect that such data would generate an expanding shock wave for $t > 0$.

However, we can observe numerically that this is not what occurs for the flow corresponding to Γ_2 . In Figure 7 we have plotted the trajectory Γ_2 from Figure 5, together with the trajectory Γ_3 , near P_9 (solid curve). We have also included the “Hugoniot-locus” H of Γ_2 (dotted curve). This is the curve of points (V_+, C_+) obtained from the Rankine-Hugoniot relations (3.1)-(3.2) as (V_-, C_-) moves down from the origin along Γ_2 . It may be deduced from the entropy condition that, for the solutions under consideration, a shock generated at collapse and propagating outward must necessarily be a 3-shock which connects the outer state (V_-, C_-) , located above \mathcal{L}_- , to the inner state (V_+, C_+) located below \mathcal{L}_- . The presence of an expanding shock would then manifest itself by H intersecting the trajectory Γ_3 at a point strictly below the critical line \mathcal{L}_- . However, Figure 7 shows that H (dotted curve) reaches P_9 without first intersecting Γ_3 : no shock is formed.

ACKNOWLEDGEMENTS

This material is based in part upon work supported by the National Science Foundation under Grant Number DMS-1813283 (Jenssen). Any opinions, findings, and conclusions or recommendations expressed in this material are those of the authors and do not necessarily reflect the views of the National Science Foundation.

The authors are grateful to Charis Tsikkou for help with the figures.

REFERENCES

- [1] S. Atzeni and J. Meyer-ter-Vehn, *The Physics of Inertial Fusion*, International Series of Monographs on Physics, vol. 125, Oxford University Press, Oxford, 2004.
- [2] Anxo Biasi, *Self-similar solutions to the compressible Euler equations and their instabilities*, Commun. Nonlinear Sci. Numer. Simul. **103** (2021), Paper No. 106014, 28, DOI 10.1016/j.cnsns.2021.106014. MR4312224
- [3] K. V. Brušlinskiĭ and Ja. M. Každan, *Self-similar solutions of certain problems in gas dynamics*, Uspehi Mat. Nauk **18** (1963), no. 2 (110), 3–23 (Russian). MR0172577
- [4] Tristan Buckmaster and Sameer Iyer, *Formation of unstable shocks for 2D isentropic compressible Euler*, Comm. Math. Phys. **389** (2022), no. 1, 197–271, DOI 10.1007/s00220-021-04271-z. MR4365141
- [5] Tristan Buckmaster, Steve Shkoller, and Vlad Vicol, *Shock formation and vorticity creation for 3d Euler*, arXiv:2006.14789 (2020).
- [6] Tristan Buckmaster, Theodore D. Drivas, Steve Shkoller, and Vlad Vicol, *Simultaneous development of shocks and cusps for 2D Euler with azimuthal symmetry from smooth data*, arXiv:2106.02143 (2021).
- [7] Demetrios Christodoulou, *The formation of shocks in 3-dimensional fluids*, EMS Monographs in Mathematics, European Mathematical Society (EMS), Zürich, 2007. MR2284927
- [8] ———, *The shock development problem*, EMS Monographs in Mathematics, European Mathematical Society (EMS), Zürich, 2019. MR3890062
- [9] R. Courant and K. O. Friedrichs, *Supersonic flow and shock waves*, Springer-Verlag, New York, 1976. Reprinting of the 1948 original; Applied Mathematical Sciences, Vol. 21. MR0421279 (54 #9284)
- [10] J. Duderstadt and G. Moses, *Inertial Confinement Fusion*, Wiley, 1982.
- [11] G. Guderley, *Starke kugelige und zylindrische Verdichtungsstöße in der Nähe des Kugelmittelpunktes bzw. der Zylinderachse*, Luftfahrtforschung **19** (1942), 302–311 (German). MR0008522
- [12] Peter Hafner, *Strong convergent shock waves near the center of convergence: a power series solution*, SIAM J. Appl. Math. **48** (1988), no. 6, 1244–1261, DOI 10.1137/0148076. MR968828
- [13] T. Hirschler and W. Gretler, *On the eigenvalue problem of imploding shock waves*, Z. Angew. Math. Phys. **52** (2001), no. 1, 151–166, DOI 10.1007/PL00001537. MR1818639
- [14] C. Hunter, *Similarity solutions for the flow into a cavity*, J. Fluid Mech. **15** (1963), 289–305, DOI 10.1017/S0022112063000252. MR153224
- [15] Helge Kristian Jenssen and Charis Tsikkou, *Amplitude blowup in radial isentropic Euler flow*, SIAM J. Appl. Math. **80** (2020), no. 6, 2472–2495, DOI 10.1137/20M1340241. MR4181105
- [16] ———, *Radially symmetric non-isentropic Euler lows: continuous blowup with positive pressure*, Submitted (2021).
- [17] Roger B. Lazarus, *Self-similar solutions for converging shocks and collapsing cavities*, SIAM J. Numer. Anal. **18** (1981), no. 2, 316–371.
- [18] Jonathan Luk and Jared Speck, *Shock formation in solutions to the 2D compressible Euler equations in the presence of non-zero vorticity*, Invent. Math. **214** (2018), no. 1, 1–169, DOI 10.1007/s00222-018-0799-8. MR3858399
- [19] ———, *The stability of simple plane-symmetric shock formation for 3D compressible Euler flow with vorticity and entropy*, arXiv:2107.03426 (2021).
- [20] Frank Merle, Pierre Raphaël, Igor Rodnianski, and Jeremie Szeftel, *On smooth self similar solutions to the compressible Euler equations*, arXiv:1912.10998 (2019).
- [21] ———, *On the implosion of a three dimensional compressible fluid*, arXiv:1912.11009 (2020).
- [22] S. Pfalzner, *An Introduction to Inertial Confinement Fusion*, Series in Plasma Physics, CRC Press, 2006.
- [23] J. Meyer-ter-Vehn and C. Schalk, *Self-similar spherical compression waves in gas dynamics*, Z. Naturforsch. A **37** (1982), no. 8, 955–969. MR676290
- [24] Scott D. Ramsey, James R. Kamm, and John H. Bolstad, *The Guderley problem revisited*, Int. J. Comput. Fluid Dyn. **26** (2012), no. 2, 79–99, DOI 10.1080/10618562.2011.647768. MR2892836
- [25] L. I. Sedov, *Similarity and dimensional methods in mechanics*, “Mir”, Moscow, 1982. Translated from the Russian by V. I. Kisin. MR693457
- [26] K. P. Stanyukovich, *Unsteady motion of continuous media*, Translation edited by Maurice Holt; literal translation by J. George Adashko, Pergamon Press, New York-London-Oxford-Paris, 1960. MR0114423
- [27] Yuxi Zheng, *Systems of conservation laws*, Progress in Nonlinear Differential Equations and their Applications, 38, Birkhäuser Boston Inc., Boston, MA, 2001. Two-dimensional Riemann problems. MR1839813 (2002e:35155)

H. K. JENSSEN, DEPARTMENT OF MATHEMATICS, PENN STATE UNIVERSITY, UNIVERSITY PARK, STATE COLLEGE, PA 16802, USA (jenssen@math.psu.edu).

A. A. JOHNSON, DEPARTMENT OF MATHEMATICS, PENN STATE UNIVERSITY, UNIVERSITY PARK, STATE COLLEGE, PA 16802, USA (axj175@psu.edu).